TALLINN UNIVERSITY OF TECHNOLOGY

FACULTY OF CHEMICAL AND MATERIALS TECHNOLOGY

DEPARTMENT OF MATERIALS SCIENCE

OXYGEN REDUCTION ON CARBON NANOMATERIAL BASED CATALYSTS

Master`s Thesis

Ragle Raudsepp

Supervisors: Ivar Kruusenberg, PhD

Kaido Tammeveski, PhD

Materials and Processes of Sustainable Energetics

2015

TALLINNA TEHNIKAÜLIKOOL

KEEMIA- JA MATERJALITEHNOLOOGIA TEADUSKOND

MATERJALITEADUSE INSTITUUT

HAPNIKU REDUTSEERUMINE SÜSINIKNANOMATERJALIDEL BASEERUVATEL KATALÜSAATORITEL

Magistritöö

Ragle Raudsepp

Juhendajad: Ivar Kruusenberg, PhD

Kaido Tammeveski, PhD

Materjalid ja protsessid jätkusuutlikus energeetikas

2015

Declaration

Hereby I declare that this master`s thesis, my original investigation and achievement, submitted for the master degree at Tallinn University of Technology has not been submitted for any degree or examination.

Ragle Raudsepp

Contents

1. Abbreviations and symbols

A - electrode geometric area

BDD – boron-doped diamond

BTDE - boron trifluoride diethyl etherate

c^b_{O2} concentration of the oxygen in the bulk

CNT – carbon nanotubes

CTAB - cetyltrimethylammonium bromide

DHP – dihexadecyl hydrogen phosphate

D_{O2} – oxygen diffusion coefficient

F – Faraday constant

FWCNT – few-walled carbon nanotubes

GC – glassy carbon

GO – graphene oxide

HOPG – highly oriented pyrolytic graphite

I - current

I_d – diffusion-limited current

I_D – disk electrode current

I_k – kinetic current

I_R – ring electrode current

j_d – diffusion-limited current density

j_k – kinetic current density

k_i – reaction rate constant

K-L - Koutecky-Levich

n – number of electrons transferred per O_2 molecule

N - collection efficiency

ORR – oxygen reduction reaction

PG – pyrolytic graphite

Q – quinone

$Q^{\bullet-}$ - quinone radical anion

r_1 – disk electrode radius

r_2 – ring electrode inner radius

r_3 – ring electrode outer radius

RDE – rotating disk electrode

RRDE – rotating ring-disk electrode

SDS – sodium dodecyl sulphate

SEM – scanning electron microscopy

SHE – standard hydrogen electrode

TEM – transmission electron microscopy

XPS – X-ray photoelectron spectroscopy

δ_d – thickness of diffusion-convection layer

ν – kinematic viscosity of the electrolyte

υ – scan rate

ω – electrode rotation rate

1BC – boron-doped carbon with a mass ratio 1/5

2BC - boron-doped carbon with a mass ratio 1/10

3BC - boron-doped carbon with a mass ratio 1/20

4BC - boron-doped carbon with a mass ratio 1/40

2. Introduction

The oxygen reduction reaction (ORR) is one of the most substantial reactions in energy-conversion systems such as fuel cells and metal-air batteries. The ORR takes place on a fuel cell cathode side and its kinetics directly affects the overall efficiency of a fuel cell [1]. Unfortunately, the kinetics of the ORR is rather slow because of the high energy demand of breaking the O=O bond (494 kJ/mol). In order to speed up the process, ORR catalyst is needed. At current technology platinum-based catalysts have shown the best catalytic activity towards the ORR. Since platinum is expensive and has many other disadvantages like dissolution and sensitivity for impurities, alternative catalyst is needed which would have the similar electrocatalytical activity to that of platinum, but could overcome mentioned drawbacks. Therefore searching non-platinum catalyst for ORR with up-mentioned properties is one of the key issues for large-scale production of fuel cells. For recent decades carbon materials have attracted a lot of attention for ORR as individual catalysts and as catalyst supports due to their low cost, good conductivity and high surface area. Many different types of carbon materials have been examined, e.g. pyrolytic graphite (PG) and highly oriented pyrolytic graphite (HOPG), glassy carbon (GC), carbon nanotubes (CNT), graphene, boron-doped diamond (BBD), etc. Since there is a vast number of different forms of carbon and the possibilities for modification is immense there is still a lot to discover in the area.

This work consists of two parts in which the first one includes preparation of surfactant coated carbon nanotubes and investigation of electrocatalytic activity of these materials towards the ORR. The second part involves synthesis of boron-doped carbon nanomaterials and studying of the ORR process on these catalysts for anion exchange membrane fuel cell (AEMFC) applications. In addition, physical characterisation of as-prepared catalyst materials were carried out using scanning electron microscopy (SEM), transmission electron microscopy (TEM), Raman spectroscopy and X-ray photoelectron spectroscopy (XPS). For electrochemical characterisation the rotating disk electrode and rotating ring-disk electrode methods were used.

3. Literature overview

3.1. Oxygen electroreduction

Oxygen electroreduction is a rather complicated reaction involving multi-electron transfer. It contains of several steps and depends on many characteristics like the type of electrode material, catalyst and electrolyte solution. In aqueous solutions the ORR has two main pathways: four-electron reduction and two-electron reduction [2]. Four-electron reduction is preferred when it comes to fuel cells and metal-air batteries because only water is produced during this reaction. Through the two-electron reduction hydrogen peroxide is produced, which accelerates fuel cell materials degradation, but is preferred in industries where production of H_2O_2 is the primary goal. Simplified O_2 reduction mechanism in acid media is illustrated on Scheme 1 [3]. Main ORR processes with corresponding thermodynamic electrode potentials at standard conditions are presented next. All the potentials are given with respect to the standard hydrogen electrode (SHE) potential, which is zero at all temperatures.

In acid aqueous electrolyte solution:

$$O_2 + 4H^+ + 4e^- \rightarrow 2H_2O \qquad\qquad 1.229 \text{ V vs. SHE} \qquad\qquad (1)$$

$$O_2 + 2H^+ + 2e^- \rightarrow H_2O_2 \qquad\qquad 0.67 \text{ V} \qquad\qquad (2)$$

Hydrogen peroxide can further reduce or catalytically decompose into water:

$$H_2O_2 + 2H^+ + 2e^- \rightarrow 2H_2O \qquad\qquad 1.76 \text{ V} \qquad\qquad (3)$$

$$2H_2O_2 \rightarrow 2H_2O + O_2 \qquad\qquad (4)$$
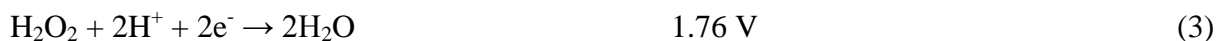
In alkaline aqueous solution:

$$O_2 + 2H_2O + 4e^- \rightarrow 4OH^- \qquad\qquad 0.401 \text{ V} \qquad\qquad (5)$$

$$O_2 + H_2O + 2e^- \rightarrow HO_2^- + OH^- \qquad\qquad -0.065 \text{ V} \qquad\qquad (6)$$

$$HO_2^- + H_2O + 2e^- \rightarrow 3OH^- \qquad\qquad 0.867 \text{ V} \qquad\qquad (7)$$

$$2HO_2^- \rightarrow 2OH^- + O_2 \qquad\qquad (8)$$

[1, 3, 4].

$$O_2 \underset{}{\overset{}{\rightleftharpoons}} O_{2(ads)} \underset{k_2}{\overset{k_1}{\rightleftharpoons}} H_2O_{2(ads)} \overset{k_3}{\longrightarrow} H_2O$$

with k_4 and k_5 pathways connecting to H_2O_2.
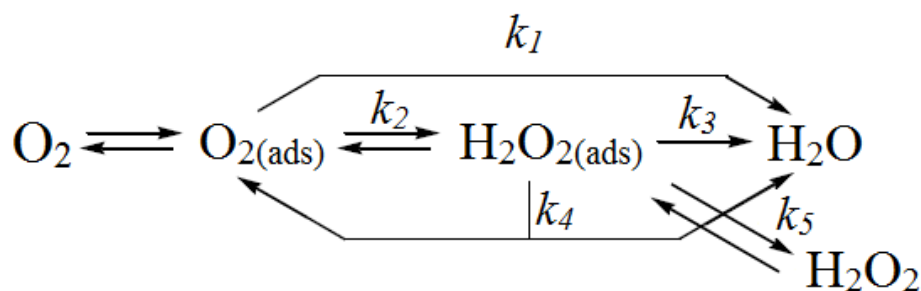
Scheme 1. Simplified mechanism of O_2 reduction in acid media, where k_i indicates reaction rate constant for different steps and (ads) demonstrates adsorbed state.

3.2. Oxygen electroreduction on bulk carbon electrodes

Since carbon materials with large surface area have been widely used as a support material for ORR catalyst a lot of interest has been shown towards carbon-based electrodes. Depending on a type of carbon material and electrolyte solution the ORR mechanism can wary widely. The ORR activity of carbon materials has been widely studied in alkaline media since most of the carbon materials exhibit good electrochemical behaviour at higher pH values [5]. Various carbon materials have been studied, such as glassy carbon (GC), pyrolytic graphite (PG), highly oriented pyrolytic graphite (HOPG), boron-doped diamond (BDD), amorphous carbon, etc. [6]. Oxygen reduction on carbon materials has a complicated mechanism and involves many steps and intermediates. Mostly two-electron electroreduction takes place on carbon electrodes but with some of the materials e.g. oxidized glassy carbon and oxidized graphite, further reduction of peroxide to water at more negative potentials is possible [7, 8]. As mentioned earlier the ORR pathway depends strongly on solution pH. It has been found that at higher pH values O_2 reduction is not that dependent on pH as it is at lower pH values [5]. The product of ORR is also dependent on pH [9]. At higher pH values this dependence occurs due to quinone groups on a carbon material [10]. It has been reported that the attachment of the quinone radical anions ($Q^{\bullet-}$) leads to enhancement of O_2 reduction [11, 12]. This is because $Q^{\bullet-}$ reacts with molecular oxygen and forms superoxide radical (O_2^-) which further reacts rather fast [10, 11].

The following ORR pathway on quinone groups has been proposed in the literature [13, 14]:

$$Q + e^- \rightarrow Q^{\bullet-} \tag{9}$$

$$Q^{\bullet-} + O_2 \rightarrow O_2^{\bullet-} + Q \tag{10}$$

$$O_2^{\bullet-} + H_2O + e^- \rightarrow HO_2^- + OH^- \tag{11}$$

$$2O_2^{\bullet-} + H_2O \rightarrow HO_2^- + O_2 + OH^- \tag{12}$$

3.3. Oxygen electroreduction on carbon nanomaterials

Since the discovery of carbon nanotubes (CNTs), a tremendous work has been done to study the material. CNTs are very unique material due to its chemical, structural, electronic and mechanical properties and therefore have received a lot of interest also among electrocatalyst studies. As mentioned before, the ORR proceeds mostly via two-electron process on carbon materials in alkaline media and hydrogen peroxide is formed, but depending on the CNT preparation method and electrode potential peroxide can be further reduced and both H_2O_2 and OH^- will be produced [15]. The ORR on CNTs strongly depends on oxygen functional groups on nanotubes surface. Matsubara and Waki showed that multi-walled carbon nanotubes (MWCNT) treated with acid exhibited better performance as ORR catalyst compared with untreated MWCNTs [16]. Although CNTs show little activity in lower pH solutions they still can be used as a catalyst support in acidic media because of their good conductivity [17, 18].

Graphene is another carbon material which has attracted a lot of attention among electrochemists. It has many advantages like good electrical conductivity, high specific surface area, chemical and thermal tolerance [19]. One of the most efficient ways to produce graphene is by thermal or chemical reduction of graphene oxide (GO). After thermal treatment of GO the oxygen-containing groups are removed from the material surface leaving defects and vacancies, which act as active sites for further treatment, e.g. heteroatom doping. For electronic applications further modification of graphene is needed while graphene itself has poor electron donor and acceptor properties [20]. Another drawback is that graphene layers tend to restack due to van der Waals interactions and therefore the number of active sites will be decreased [21]. In order to overcome these mentioned barriers and to enhance graphene electrochemical properties, carbon nanotubes have been introduced to the graphene material as separators [22-28]. Choi et al. demonstrated that in the CNT and graphene assembly nanotubes performed as circuits for electron transfer and as separators for preventing graphene sheets to restack [27].

3.4. Oxygen electroreduction on heteroatom-doped carbon nanomaterials

Doping carbon materials with heteroatoms changes their electronic properties and has found to be an easy and effective way to improve the ORR kinetics [29, 30]. Heteroatom-doped carbon materials are attractive due to their low cost, superior tolerance to fuel impurities, long term stability, good electrocatalytic activity towards the ORR and environmental friendliness [29-32]. Mostly N, P, S and B doping have been studied because of their reasonable atomic

size in order to enter into carbon network [29, 33-37]. It has been demonstrated that by introducing atoms with different electronegativity than the host atomic network, the electroneutrality of the material will be broken and therefore favourable adsorption sites for O_2 are created [38]. O_2 molecule, which is slightly negatively charged while approaching the carbon network, favours adsorption on the positively charged sites, which is carbon connected to the nitrogen or phosphorous dopant and boron in boron-doped carbon material [39-41]. Most examined heteroatom doped materials are different forms of carbon like single-, double- and multi-walled carbon nanotubes, graphene and nanodiamonds [28, 38, 42-46].

Nitrogen-doped carbon materials have been most extensively studied in comparison to the other catalysts doped with other heteroatoms [28, 39, 47-50]. Based on previous investigation results, nitrogen atom can be incorporated into carbon network in the form on pyridinic-, pyrrolic-, graphitic- or quarternary-N [51]. It has been proposed that the biggest role in catalytic activity plays graphitic- and pyridinic-N species, which accelerate O_2 reduction and promote four-electron electroreduction [52].

Recent studies show that also phosphorus-doped carbon materials exhibit enhanced catalytic activity towards the ORR compared with non-doped materials [53]. It is suggested that in carbon network phosphorous has good electron-donating properties and therefore increases electron delocalization in the material which creates active sites for ORR [54]. Although P-doping improves material electrocatalytic activity it is mostly used as co-dopant with nitrogen. Choi, et al. showed that additional P-doping increased N-doped carbon material activity for 108% [29].

3.4.1. Oxygen electroreduction on boron-doped carbon nanomaterials
In recent years boron-doped materials have caught a lot of interest and it has been found to have even slightly better electrocatalytic properties than N-doped materials [55].

There are several methods for doping boron into carbon network: *i)* chemical vapour deposition, *ii)* thermal annealing, *iii)* two-step thermal treatment and *iv)* single-step pyrolysis [31, 32, 38, 44, 46, 56, 57]. Some of these methods can be quite complicated while involving several steps and a presence of catalysts. On the other hand pyrolysis is effective and rather facile method for boron-doping.

Lazar et al. demonstrated that depending on the chemical nature of doping, boron can be added into carbon network by substitutional or additive doping [43]. After substitutional doping boron will be bonded to carbon sp^2 network by replacement of carbon atoms within

the carbon structure [57]. As a result the host network acquires p-type conductivity [53, 58]. Additive doping introduces sp^3 carbon atoms into sp^2 carbon network while BH_2 species are added on the surface and on the edge of carbon material [43]. From thermodynamic point of view substitutional doping is preferred more than additive while transforming sp^2 in-plane carbon to sp^3 out-plane carbon requires a lot of energy [43]. Most common bonding configurations of boron incorporated into carbon network are BCO_2, BC_2O, BC_3 and B_4C [29, 31, 32, 46, 57, 59]. Jo and Shanmugam demonstrated that the catalyst which contained higher amount of B_3C, B_4C and BC_3 species was more active towards the ORR [32]. This indicates that higher B/C ratio is driving force to enhance the ORR kinetics, which was also showed by Cheng et al. [46].

Yang et al. showed that positively charged boron atoms promote chemisorption of O_2 and then act as a bridge from which electrons from adjacent carbon atoms move to chemosorbed O_2 which weakens the O-O bond and leads to the ORR process [38]. Fazio et al. demonstrated that on a B-doped graphene associative oxygen reduction is preferred rather than dissociative [45]. This means that after the adsorption of O_2, end-on dioxygen species (BGOO) are formed, which will be directly reduced to hydroperoxo species (BGOOH) without going through energetically expensive side-on intermediate as it is with the dissociative mechanism [45].

3.5. Oxygen electroreduction on carbon nanotubes modified with surfactants

While carbon nanotubes have hydrophobic nature it is difficult to obtain uniform dispersion in aqueous solvents. This means that they tend to form agglomerates, which in turn decreases material surface area and therefore catalytic activity decreases. There are two ways to get better dispersion of carbon nanotubes, one is mechanical and other is chemical approach. Mechanical approach involves ultrasound bath and high-share mixing, but these methods can be quite time consuming and ultrasound can lead to disintegration of nanotubes [60]. Chemical method includes covalent and non-covalent approaches in which the first one includes chemical reaction which can change nanotubes initial properties [61]. Non-covalent method on the other hand includes adsorption onto the nanotube surface and electronic properties of nanotubes will remain unchanged. Both polymers and surfactants are used to disperse carbon nanotubes by non-covalent chemical methods. For electronic applications polymers are not suitable while they can also participate in charge delocalisation and therefore alter electronic properties of the material [62]. Using surfactants is easy and effective way to

disperse carbon nanotubes. There are three different types of surfactants which can be used – non-ionic, cationic and anionic surfactants. Non-ionic surfactants adsorb onto carbon surface through π-π stacking interactions and charged surfactants through Coulomb attraction [63]. The enhanced dispersion occurs due to electrostatic repulsion in the presence of ionic surfactant and due to steric effect in the presence of non-ionic surfactant [64]. It has been demonstrated that there is an optimum amount of surfactant that can be adsorbed on the nanotube surface and if this amount is exceeded charge transfer within CNT network will be affected [65].

3.6. Methods for electrochemical characterization

3.6.1. Rotating disk electrode method

The rotating disk electrode (RDE) method is one of the most frequently used methods for studying kinetics and mechanism of electrochemical reactions. Its main advantage is that the rate of mass transport to the RDE surface is uniform. During the rotation the electrolyte solution is dragged onto the surface of RDE while centrifugal force pushes the electrolyte solution away from the centre. This flow of electrolyte is supplemented by a flow normal onto the RDE surface and therefore during the rotation the flow rate towards the electrode and around it is laminar [2]. Since the solution flow towards the electrode is laminar the rate of mass transport can be calculated using Levich equation [2]:

$$j_d = 0.62nFc_{O_2}^b D_{O_2}{}^{2/3}\nu^{-1/6}\omega^{1/2} \tag{13}$$

where j_d is the diffusion-limited current density, n is the number on electrons transferred per O_2 molecule, F is the Faraday constant (96,485 C/mol), D_{O2} is the diffusion coefficient of oxygen (cm^2/s), and $c^b{}_{O2}$ is the O_2 concentration in the bulk (mol/cm^3), ν is the kinematic viscosity of the electrolyte (cm^2/s), ω is the rotation rate (rad/s). Based on this theory the limiting current is a linear function of the reagent concentration and therefore it is possible to calculate the diffusion coefficient of the reacting species.

Usually measured currents follow the mixed kinetic case and therefore diffusion-limited current density and the kinetic current densities both have to be taken into account.

$$j_k = \frac{j_d j}{j_d - j} \tag{14}$$

j_k is the kinetic current density.

The Koutecky-Levich (K-L) equation can be used to calculate the number of electrons transferred per O_2 molecule:

$$\frac{1}{I} = \frac{1}{I_k} + \frac{1}{I_d} = -\frac{1}{nFAkC_{O_2}^{\ b}} - \frac{1}{0.62nFAD_{O_2}^{2/3} v^{-1/6} c_{O_2}^{b} \omega^{1/2}} \tag{15}$$

where I is measured current, I_k and I_d are kinetic and diffusion-limited currents, respectively, k is the rate constant for oxygen reduction, A is electrode geometric area, F is the Faraday constant (96,485 C/mol), D_{O2} is the diffusion coefficient of oxygen (cm^2/s), $c_{O2}^{\ b}$ is the concentration of the oxygen in the bulk (mol/cm^3), v is the kinematic viscosity of the electrolyte (cm^2/s) and ω is the rotation rate (rad/s). From the slope of K-L lines the number of electrons transferred per O_2 molecule or diffusion coefficient can be found. Also exchange current density and the electron transfer coefficient can be found from the intercept of K-L plot [66].

3.6.2. Rotating ring-disk electrode method

In electrochemistry the rotating ring-disk electrode (RRDE) method is a powerful tool especially when intermediate compounds are needed to detect. While RDE consists of one disk electrode then RRDE consists of one disk electrode and a ring electrode, which both work independently. Difference between RDE and RRDE comes in when centrifugal force pushes the electrolyte solution away from the centre which now moves to ring electrode where quantitative analysis of reaction products is taking place. Important parameters are the disk radius and the ring inner and outer radius.

For quantitative measurements of disk reaction products, parameter called collection efficiency has to be found using the following equation [4]:

$$N = 1 - F\left(\frac{r_2^3 - r_1^3}{r_3^3 - r_2^3}\right) + \left(\frac{r_3^3 - r_2^3}{r_1^3}\right)^{\frac{2}{3}}\left[1 - F\left(\left(\frac{r_2}{r_1}\right)^3 - 1\right)\right] - \left(\frac{r_3}{r_1}\right)^2\left\{1 - F\left[\left(\frac{r_2^3 - r_1^3}{r_3^3 - r_2^3}\right)\left(\frac{r_3}{r_1}\right)^3\right]\right\} \tag{16}$$

where N is collection efficiency, r_1 is disk electrode radius, r_2 and r_3 are ring electrode inner and outer radius, respectively.

Equation (16) demonstrates that by increasing the ring electrode area the collection efficiency increases.

The percentage of produced H_2O_2 can be calculated using the equation:

$$\%_{H_2O_2} = \frac{2I_R/N}{I_D + I_R/N} \times 100 \tag{17}$$

where I_D is disk electrode current and I_R is ring electrode current.

The value of n can be also calculated from the RRDE data:

$$n = \frac{4I_D}{I_D + I_R/N} \tag{18}$$
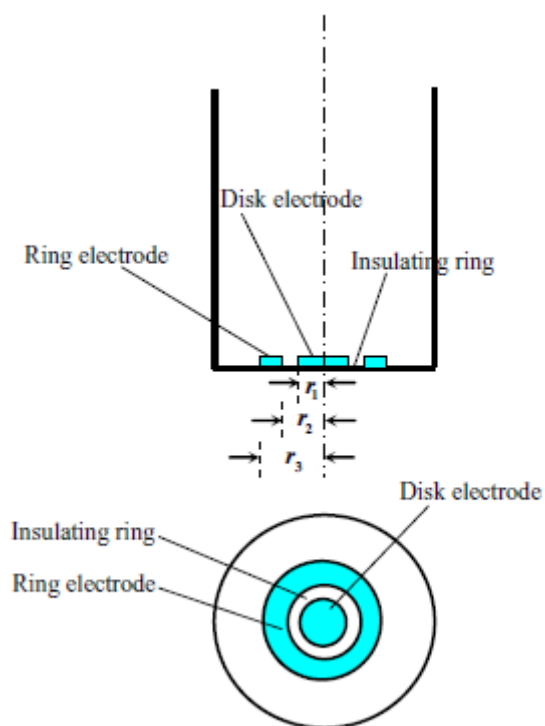
Scheme 2. Rotating ring-disk electrode [2].

4. Experimental

4.1. Preparation of surfactant coated FWCNTs

Over 99.6 wt% pure few-walled carbon nanotubes (FWCNT) received from Noda Lab (Japan) was used as a carbon nanotube material and several surfactants were used as modifying agents. Octylphenoxypolyethoxyethanol (Triton X-100), cetyltrimethylammonium bromide (CTAB), sodium dodecyl sulphate (SDS) and dihexadecyl hydrogen phosphate (DHP) were all purchased from Sigma-Aldrich.

FWCNTs were mixed with ethanol and Milli-Q water (Millipore, Inc.) and lastly surfactant was added. Triton X-100 concentration in the mixture was 0.3%, CTAB was 0.3%, SDS was 1% and DHP was 0.1%, with these concentrations the critical micelle concentration was exceeded [64]. Mixtures were sonicated for 1.5 h in ultrasound bath and then left to magnetic stirrer for overnight in order to get better dispersion.

4.2. Preparation of B-doped carbon nanomaterials

The FWCNTs were mixed with GO, which was synthesised from graphite powder (Graphite Trading Company) by modified Hummers`method [67, 68]. Boron trifluoride diethyl etherate (BTDE) (Sigma Aldrich) was used as boron source for doping. Firstly, the FWCNTs were oxidized at room temperature in a mixture of 1:1 H_2SO_4 and HNO_3 solution in order to introduce defects and oxygen functional groups on a surface, which in turn increases the probability of boron doping of CNTs.

Pyrolysis method was used to synthesise B-doped carbon nanomaterials. The FWCNTs and GO with a ratio of 1:1 were mixed with a BTDE. Four different mass ratios were prepared (FWCNT and GO/boron source = 1/5, 1/10, 1/20 and 1/40) and designated as 1BC, 2BC, 3BC and 4BC, respectively. All the mixtures were sonicated for 1 h, then placed into quartz boat and dried in a vacuum oven at 70 °C for 30 min. Materials were pyrolysed in argon atmosphere at 800 °C at a rate of 7 °C/min for 2 h and then cooled to a room temperature. For comparison purposes also pyrolysis at 600 °C and 1000 °C were carried out with the catalyst material mixture which carbon/boron mass ratio exhibited best catalytic activity at 800 °C.

4.3. Physical characterisation of prepared catalyst materials

X-ray photoelectron spectroscopy (XPS) was used to analyse surface composition of as synthesized B-doped carbon nanomaterial. Catalyst material was suspended in ethanol and deposited on a polished glassy carbon (GC) plate (1.1 × 1.1 cm) after which the plate was dried in vacuum oven at 70 °C. Electron energy analyser (SCIENTA SES100) and non-

monochromatic twin anode X-ray tube (XR3E2) with characteristic energies of 1253.6 eV (Mg $K_{\alpha1,2}$, FWHM 0.68 eV) and 1486.6 eV (Al $K_{\alpha1,2}$, FWHM 0.83 eV) were used for XPS studies. Pressure in the analysis chamber was below 10^{-9} Torr. To collect the survey scan the energy range from 800 to 0 eV, pass energy 200 eV and step size 0.5 eV was applied. For obtaining high resolution spectra at certain regions pass energy of 200 eV with step of 0.1 eV was applied.

To examine the surface morphology of nanocarbon catalysts, scanning electron microscope (SEM) Helios NanoLab 600 was used. Catalyst material was suspended in ethanol and pipetted onto a polished GC disk. Several different areas of the sample were examined in order to receive the average characteristics.

To examine catalyst material at near atomic level, transmission electron microscope (TEM) Tecnai 12, was used. Measurements were carried out at a 120 kV accelerating voltage. 300 mesh copper grid (Agar Scientific) which was coated with carbon, was used as a substrate for catalyst solution.

Raman spectra of the as prepared catalyst material was collected using spectrometer (Renishaw inVia). Ar^{+} laser with wavelength of 514 nm was used for excitation. Laser beam was focused into a spot approximately 1 μm of diameter and signal was collected with CCD detector.

4.4. Preparation of modified GC electrodes and electrochemical measurements

The electrochemical measurements were performed with a standard three-electrode system using the rotating disk electrode (RDE) method. Saturated calomel electrode (SCE) was used as a reference electrode and Pt foil was used as a counter electrode. GC disk (GC-20SS, Tokai Carbon) with a geometric area of 0.2 cm^{2} was used as a working electrode. GC disks were pressed into Teflon holder and polished to a mirror finish using aluminium oxide slurry (Buehler) with a grain size of 1 μm. After polishing the electrodes were sonicated in Milli-Q water and isopropanol both for 5 min.

For electrode preparation with surfactant-modified carbon nanotubes, 0.05 mg/cm^{2} of catalyst material was dropped onto the GC surface and dried in oven at 70 °C for 30 min. Measurements were carried out using four different surfactants in three different electrolyte solutions with different pH value. 0.1 M KOH (pH = 13), 0.1 M phosphate buffer (pH = 7) and 0.5 M H_2SO_4 (pH = 0.3) electrolytes were used.

For electrode preparation with B-doped carbon material, the as-prepared doped material was suspended in isopropanol (4 mg/ml) containing 0.25% Tokuyama ionomer AS-4. 20 µl of the prepared catalyst solution was dropped onto the polished GC surface and then dried at 70 °C in vacuum oven for 30 min. Measurements were carried out in O_2 saturated 0.1 M KOH (Merck) solution.

The electrode rotation rate (ω) was varied from 360 to 4600 rpm using EDI101 rotator (Radiometer) and speed control unit CTV101. Potential was applied using Autolab potentiostat PGSTAT30 (Eco Chemie B.V., The Netherlands) and experiment was controlled by using General Purpose Electrochemical System (GPES) software. The prepared catalyst material activity was evaluated by cyclic voltammetry (CV) and linear sweep voltammetry (LSV) measurements, with the scan rate of 100 mV/s and 10 mV/s respectively.

Also the RRDE measurements were carried out with FWCNTs materials. As received FWCNTs were mixed with ethanol and mixture was dispersed in ultrasound bath for 1.5 h. GC disk with Pt ring and geometric area of 0.2 cm^2 was used as a working electrode (Pine Research Instrumentation, Inc., Grove City, PA, USA). GC disk was pressed into Teflon holder and polished to a mirror finish using alumina slurry (Buehler) with grain size of 1 µm. After polishing the electrode was sonicated in acetonitrile (Sigma-Aldrich), isopropanol and Milli-Q water for 5 min. Measurements with three different loading (0.05, 0.1 and 0.2 mg/cm^2) of the catalyst material were carried out in O_2 saturated 0.1 M KOH solution with a scan rate of 10 mV/s. Rotation rate was varied from 360 to 3100 rpm.

5. Results and discussion

5.1. Oxygen reduction on FWCNT modified GC electrodes

5.1.1. Physical characterisation of FWCNTs

Scanning electron microscopy (SEM) was used to investigate the surface morphology of FWCNTs. From Fig. 1 one can see that nanotubes are rather well dispersed, average diameter of nanotubes is approximately 10 nm and no visible amorphous carbon particles or other impurities can be detected.
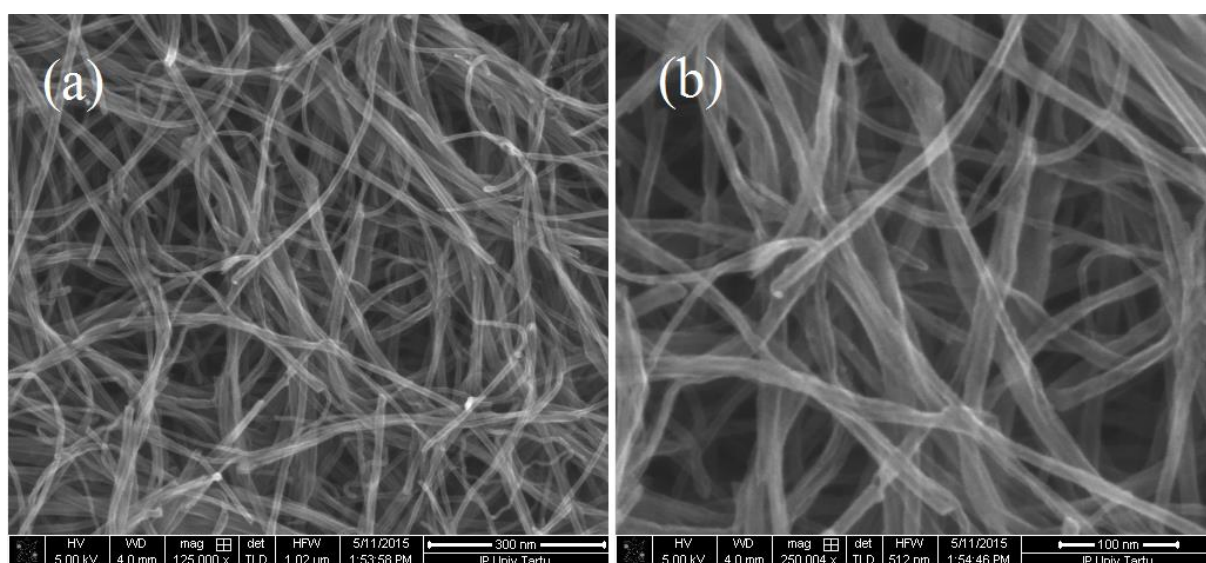
Figure 1. SEM image of Noda FWCNTs deposited on glassy carbon disk electrode.

5.1.2. Electrochemical characterisation of FWCNT/GC electrodes

RRDE method was used to study oxygen reduction on ultrapure FWCNT-modified electrodes. Measurements were carried out in O_2 saturated 0.1 M KOH solution with a scan rate of 10 mV/s and in a potential range from 0 to -1.2 V. The amount of catalyst material on the electrode surface was varied as follows: 0.05, 0.1 and 0.2 mg/cm^2. Figures 2-4 illustrate the electrochemical ORR behaviour on FWCNT modified GC electrodes, with the amount of 0.05, 0.1 and 0.2 mg/cm^2 respectively. It can be seen that no significant change in the ORR activity with different loading of catalyst material can be detected. The onset potential in all cases is approximately -0.25 V. The reduction current increases while increasing the rotation rate of an electrode and prewave is formed at a potential of -0.5 V. It can be assumed that the prewave is contributed by oxygen functional groups on nanotube surface. The amount of H_2O_2 produced on the FWCNTs is measured on the platinum ring of the RRDE. Detected amount of H_2O_2 increases when electrode rotation rate increases because at higher rotation

rates H_2O_2 moves faster from disk electrode to ring electrode and therefore has less time to be further reduced or decomposed. The percentage of H_2O_2 produced was calculated using the equation (16).

The number of electrons transferred per one O_2 molecule was calculated using Koutecky-Levich (K-L) equation (15). K-L plots on Figures 2-4 (b) indicate that ORR on FWCNT/GC in under diffusion-convection limited current at lower rotating rates and under diffusion-limited current at higher rotating rates. From the inset graphs (see Fig. 2-4 (b)) can be seen that the number of electrons transferred per O_2 molecule is approximately two in all measured potential range and for all different catalyst loadings.
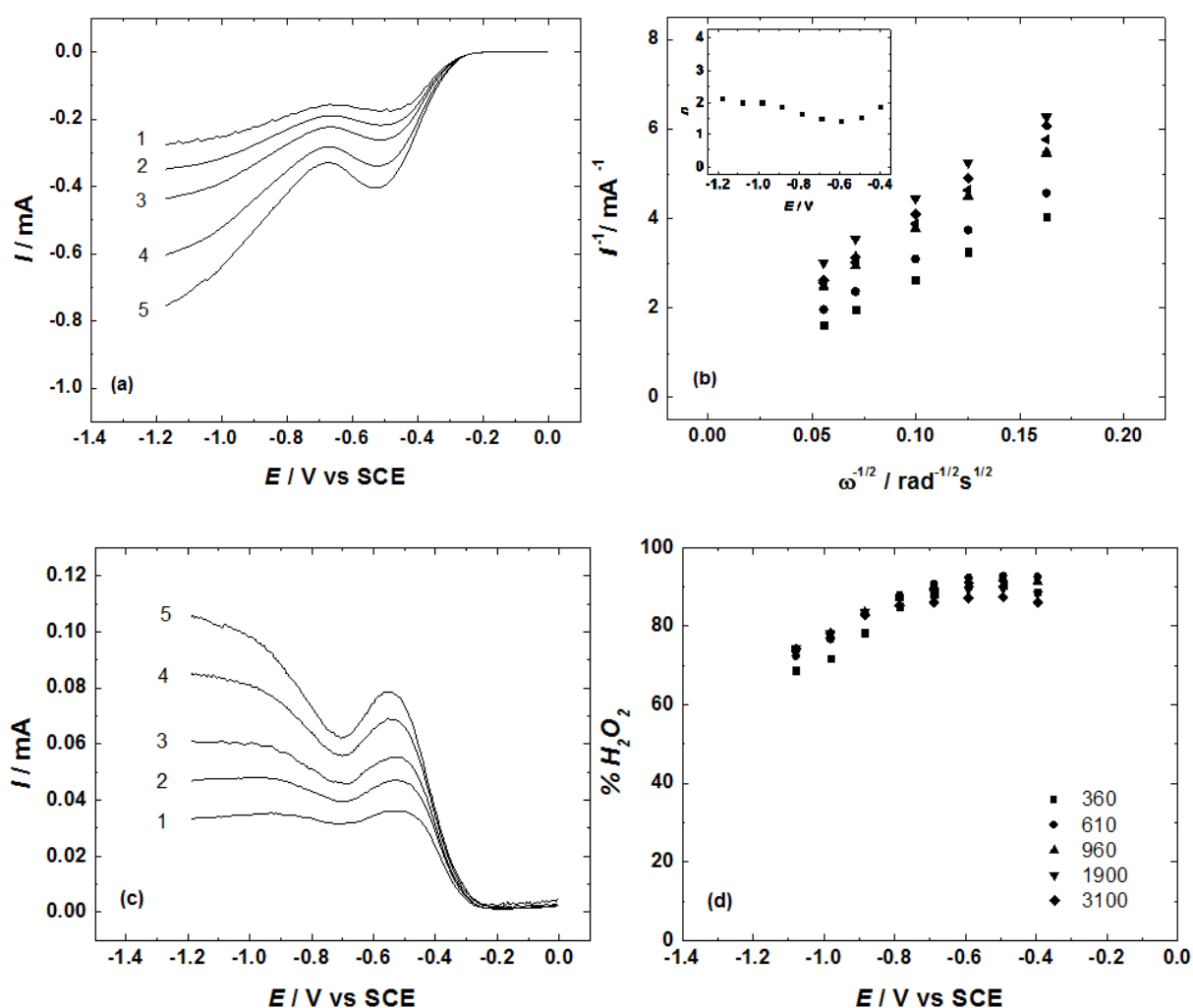
Figure 2. (a) RRDE voltammetry curves of oxygen reduction on a FWCNT/GC electrode, (b) K-L plots with inset graph illustrating number of electrons transferred per O_2 molecule, (c) ring electrode current-potential curves and (d) the percentage of H_2O_2 produced. The loading of catalyst on the electrode was 0.05 mg/cm^2. Measurements were carried out in O_2 saturated 0.1 M KOH, υ = 10 mV/s, ω = (1) 360, (2) 610, (3) 960, (4) 1900, (5) 3100 rpm. In K-L plots symbols correspond to different potentials: (■) -1.2 V, (●) -1.1 V, (▲) -1.0 V, (▼) -0.9 V, (◆) -0.8 V, (◄) -0.7 V.

Figure 3. (a) RRDE voltammetry curves of oxygen reduction on a FWCNT/GC electrode, (b) K-L plots with inset graph illustrating number of electrons transferred per O_2 molecule, (c) ring electrode current-potential curves and (d) the percentage of H_2O_2 produced. The loading of catalyst on the electrode was 0.1 mg/cm^2. Measurements were carried out in O_2 saturated 0.1 M KOH, v = 10 mV/s, ω = (1) 360, (2) 610, (3) 960, (4) 1900, (5) 3100 rpm. In K-L plots symbols correspond to different potentials: (■) -1.2 V, (●) -1.1 V, (▲) -1.0 V, (▼) -0.9 V, (◆) -0.8 V, (◄) -0.7 V.

Figure 4. (a) RRDE voltammetry curves of oxygen reduction on a FWCNT/GC electrode, (b) K-L plots with inset graph illustrating number of electrons transferred per O_2 molecule, (c) ring electrode current-potential curves and (d) the percentage of H_2O_2 produced. The loading of catalyst on the electrode was 0.2 mg/cm^2. Measurements were carried out in O_2 saturated 0.1 M KOH, $v = 10$ mV/s, $\omega = $ (1) 360, (2) 610, (3) 960, (4) 1900, (5) 3100 rpm. In K-L plots symbols correspond to different potentials: (■) -1.2 V, (●) -1.1 V, (▲) -1.0 V, (▼) -0.9 V, (◆) -0.8 V, (◄) -0.7 V.

5.2. Oxygen reduction on FWCNT-surfactant modified GC electrodes

5.2.1. Electrochemical characterisation of FWCNT-surfactant modified electrodes in alkaline media

Several different surfactants were used to achieve better dispersion of carbon nanotubes and electrocatalytic properties of these surfactant covered FWCNTs were investigated. Triton X-100 was used as a non-ionic surfactant, CTAB as a cationic surfactant, SDS and DHP as anionic surfactants. From Fig. 5 one can see that the reduction current values have increased compared with ORR on FWCNTs without the surfactant (for example, see Fig. 2). This

indicates that the specific surface area of the electrode has been increased by avoiding natural agglomeration of the CNTs. It is also obvious that dispersibility of FWCNTs has been enhanced compared with unmodified FWCNTs. In Fig. 5, K-L plots are presented and it can be seen that the K-L lines are not parallel which indicates that the number of electrons transferred per O_2 molecule (n) is not the same in studied potential range. This can also be seen from the inset graphs of Fig. 5 (b), (d), (f) and (h) that the n value increases at more negative potentials. At lower overpotentials the value of n is two and H_2O_2 is produced during the reaction. At more negative potentials the n value increases, which shows that H_2O_2 further reduces to water.
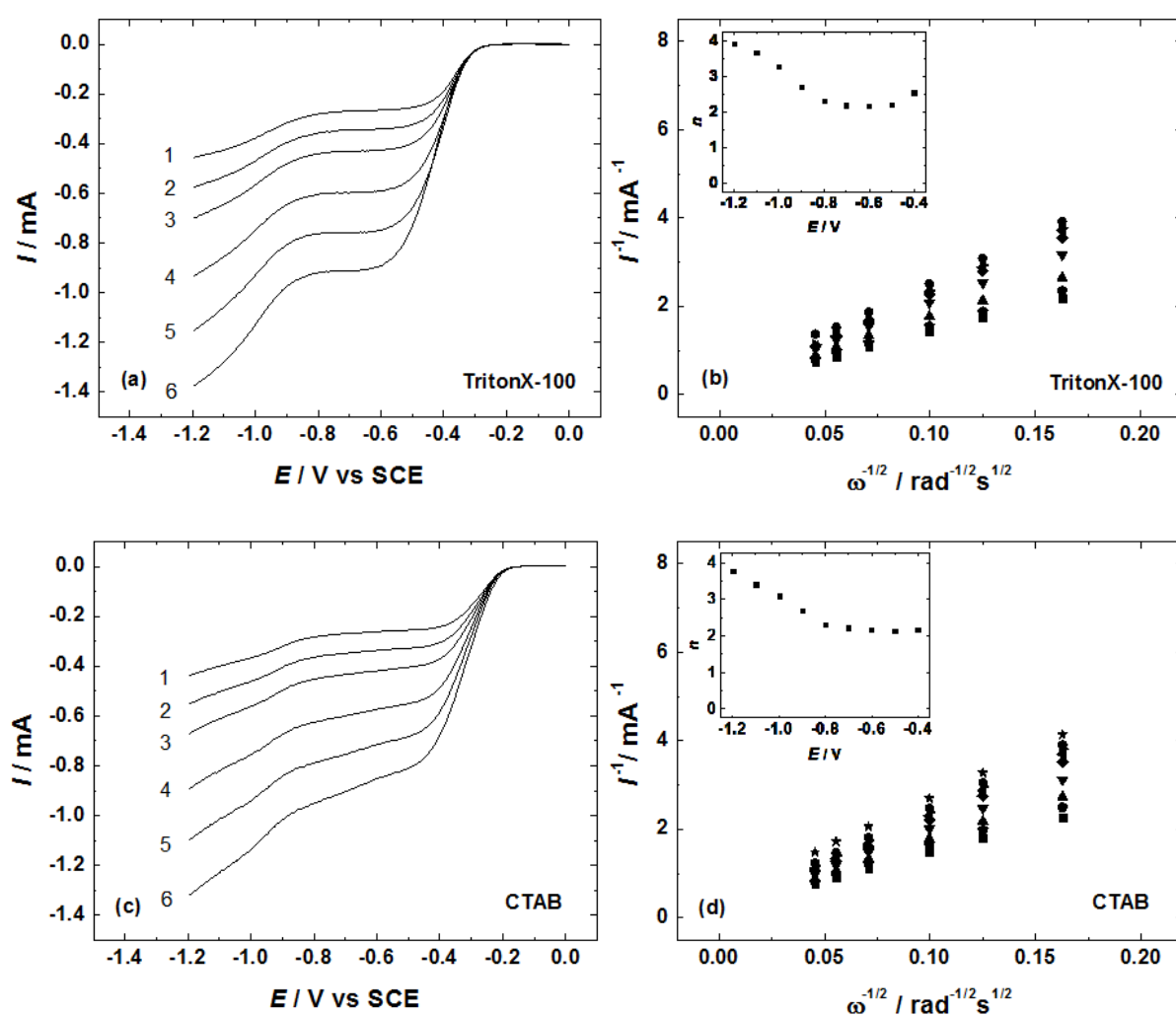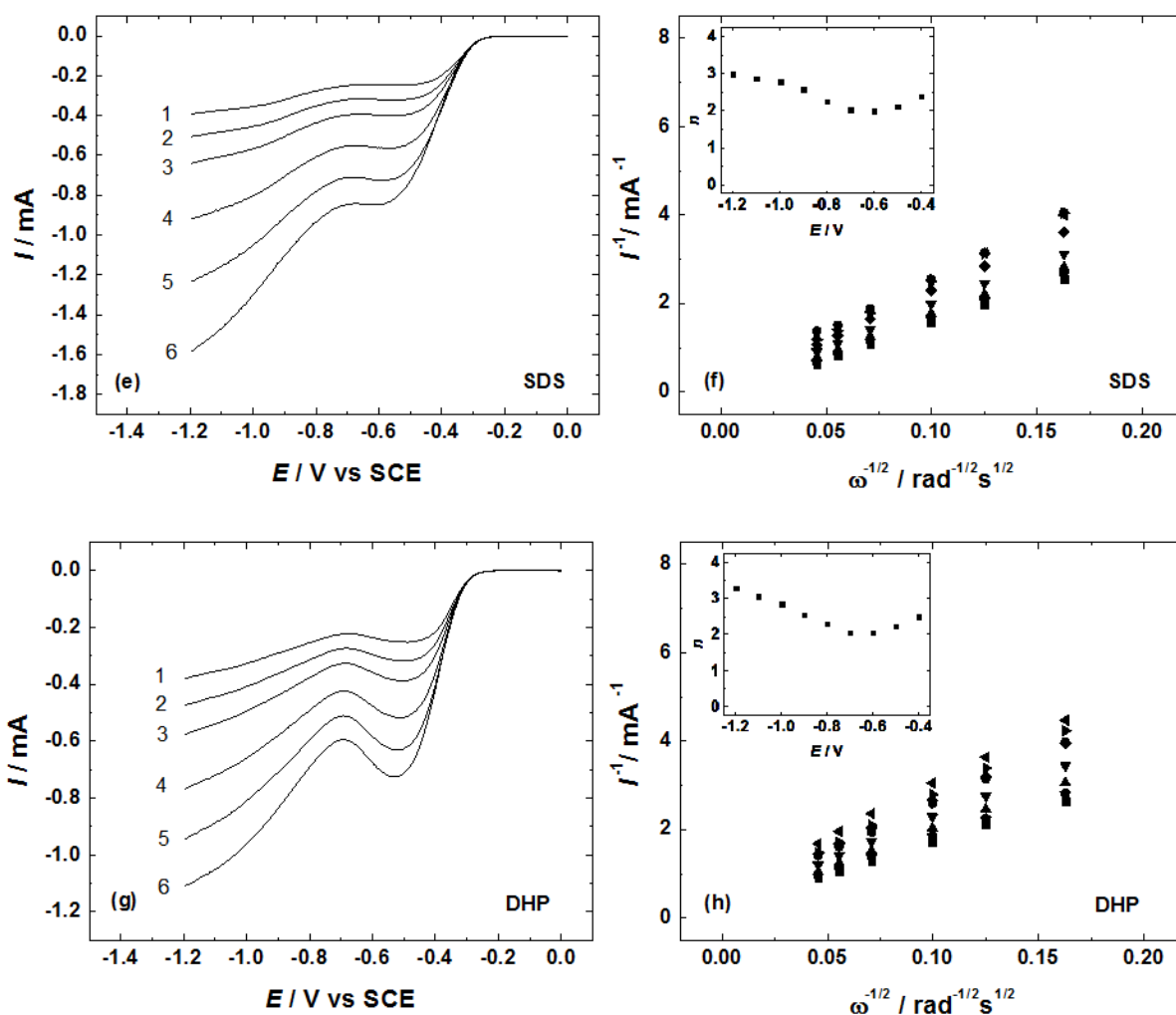
Figure 5. ORR polarisation curves and K-L plots on FWCNT-surfactant modified GC electrodes. Inset graphs show the potential dependence of the number of electrons transferred per O_2 molecule. Measurements were carried out in O_2 saturated 0.1 M KOH, $\upsilon = 10$ mV/s, ω = (1) 360, (2) 610, (3) 960, (4) 1900, (5) 3100, (6) 4600 rpm. In K-L plots symbols correspond to different potentials: (■) -1.2 V, (⬠) -1.1 V, (▲) -1.0 V, (▼) -0.9 V, (◆) -0.8 V, (◀) -0.7 V, (▶) -0.6 V, (●) -0.5 V, (★) -0.4 V.

Fig. 6 shows that FWCNTs modified with CTAB has the most positive onset potential compared with other surfactant-modified FWCNTs, unmodified FWCNTs and bare GC electrode. This could be because of FWCNTs modified with CTAB had most even dispersion compared with other surfactant containing mixtures. FWCNT modified with DHP has the lowest current values and can be said that among these four surfactants DHP showed the lowest dispersing ability.
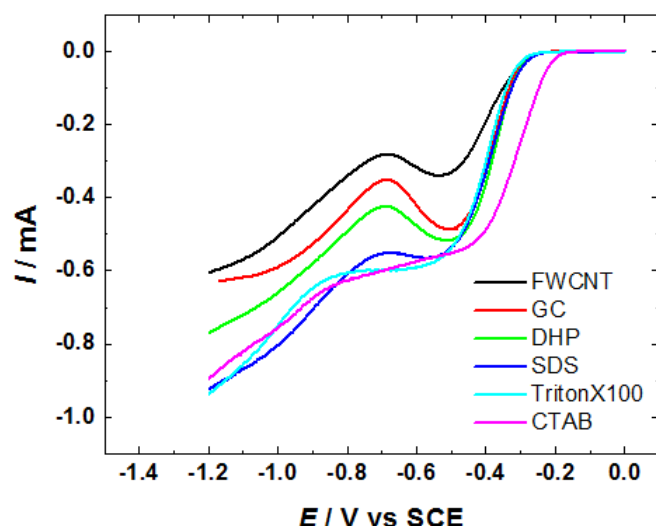
Figure 6. Comparison of the RDE voltammetry curves for ORR on a bare GC and on a FWCNT and FWCNT-surfactant modified GC electrodes. Measured in O_2 saturated 0.1 M KOH, $v = 10$ mV/s, $\omega = 1900$ rpm.

5.2.2. Electrochemical characterisation of FWCNT-surfactant modified electrodes in neutral media

Oxygen reduction on FWCNT-surfactant modified GC electrodes was also studied in 0.1 M phosphate buffer solution with pH = 7 (see Fig. 7). As it was expected, at lower pH values the electrocatalytic activity of modified carbon nanotube catalyst decreases while the nature of active sites on FWCNTs change. From Fig. 7 (b), (d), (f) and (h) inset graphs, it can be seen that unlike from the electrocatalytic behaviour in alkaline media the number of electrons transferred per O_2 molecule is two in the whole studied potential range and does not increase at more negative potentials, meaning that H_2O_2 is the final product and does not reduce further to water.
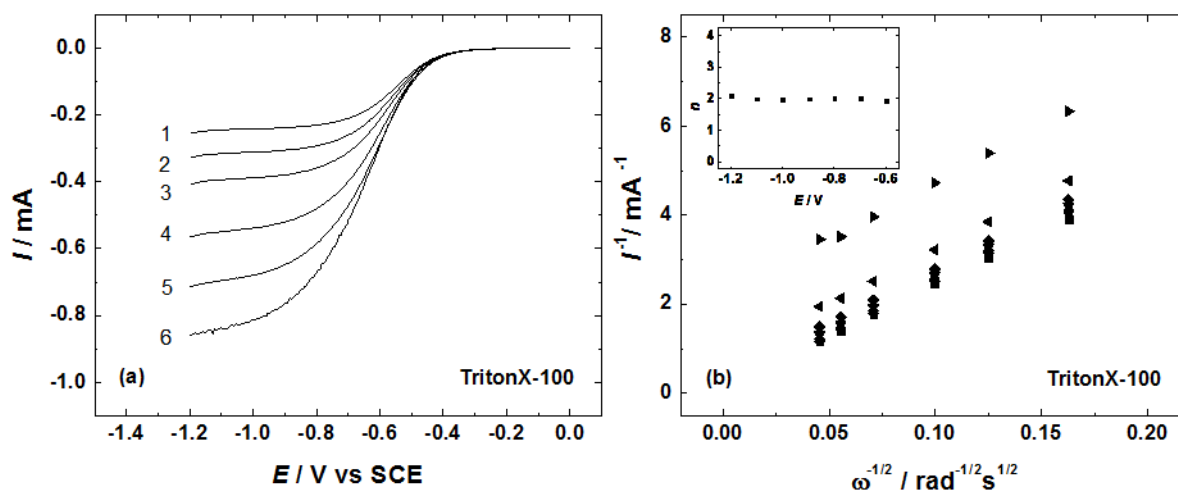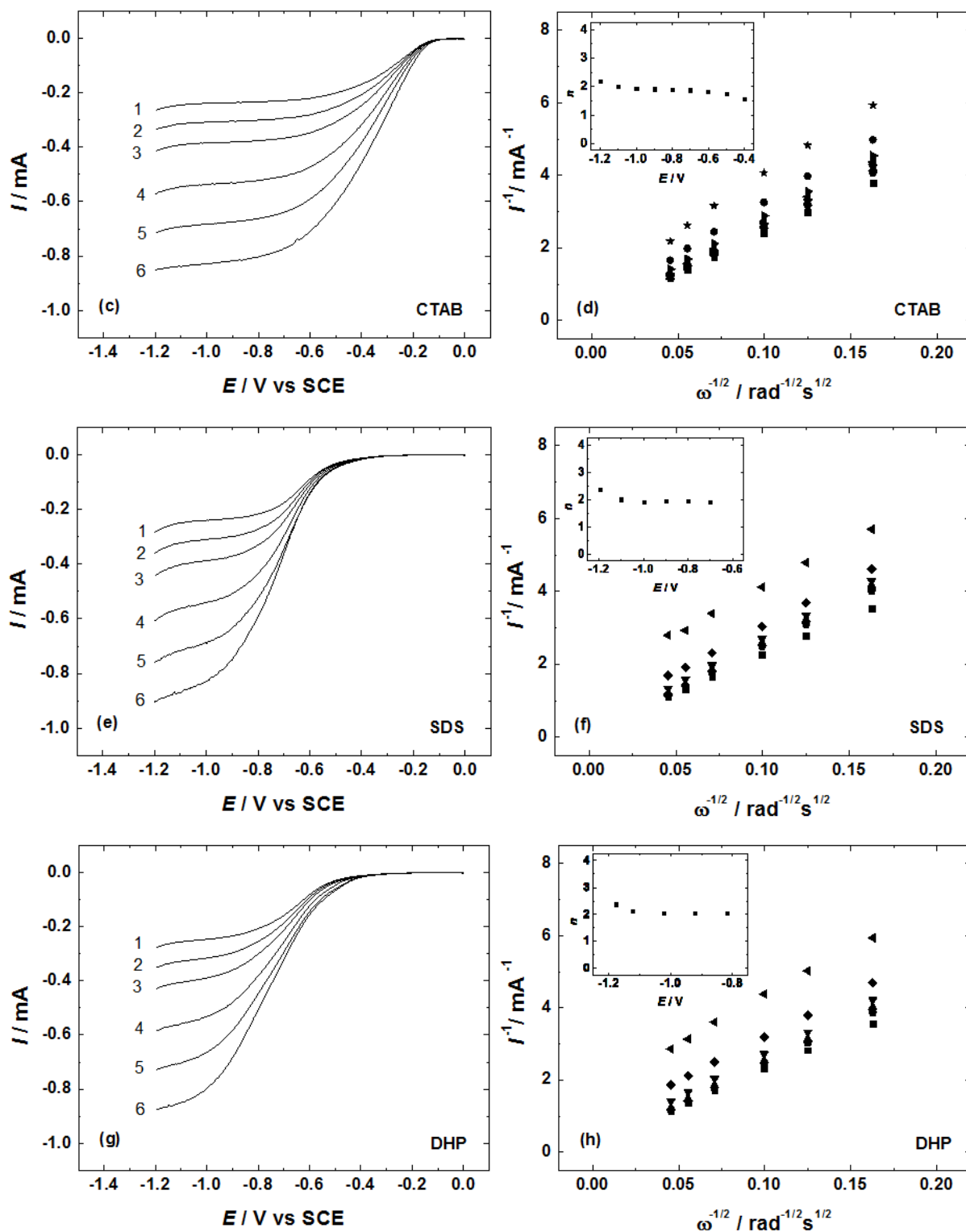
Figure 7. ORR polarisation curves and K-L plots for FWCNT-surfactant modified GC electrode. Inset graphs shows the potential dependence of the number of electrons transferred per O_2 molecule. Measurements were carried out in O_2 saturated 0.1 M phosphate buffer, v = 10 mV/s, ω = (1) 360, (2) 610, (3) 960, (4) 1900, (5) 3100, (6) 4600 rpm. In K-L plots symbols correspond to different potentials: (■) -1.2 V, (⬟) -1.1 V, (▲) -1.0 V, (▼) -0.9 V, (◆) -0.8 V, (◀) -0.7 V, (▶) -0.6 V, (●) -0.5 V, (★) -0.4 V.

From Fig. 8 it can be seen that FWCNTs modified with CTAB has the most positive onset potential compared with other surfactant-modified FWCNTs, unmodified FWCNTs and bare GC electrode, referring to better dispersion of FWCNTs in the presence of CTAB. The same situation was also detected in alkaline media (see Fig. 6).
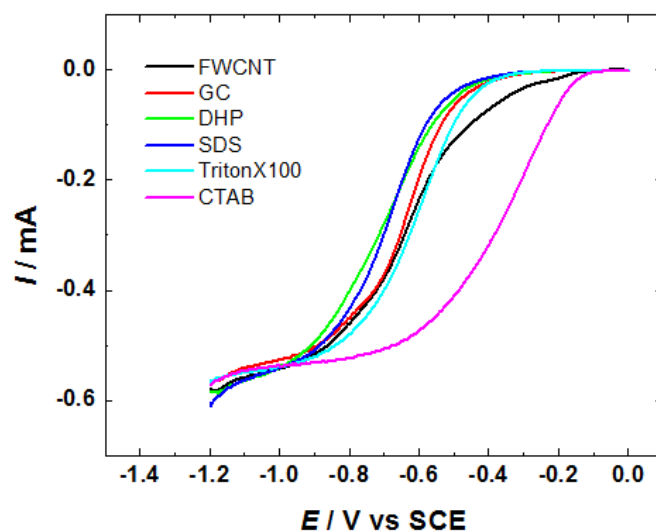
Figure 8. Comparison of the RDE voltammetry curves for ORR on a bare GC and on a FWCNT and FWCNT-surfactant modified GC electrodes. Measured in O_2 saturated 0.1 M phosphate buffer, $v = 10$ mV/s, $\omega = 1900$ rpm.

5.2.3. Electrochemical characterisation of FWCNT-surfactant modified electrodes in acid media

Electrocatalytic ORR behaviour of FWCNT-surfactant modified GC electrode was also studied in acidic media. As it was mentioned before, carbon materials exhibit rather poor electrocatalytic activity towards the ORR in acidic media, which can also be seen from Fig. 9. From these studies it can be said that in a potential range from 0.8 to -0.1 V the FWCNT material can be used as a catalyst support while having good conductivity but does not contribute to catalytic activity itself.
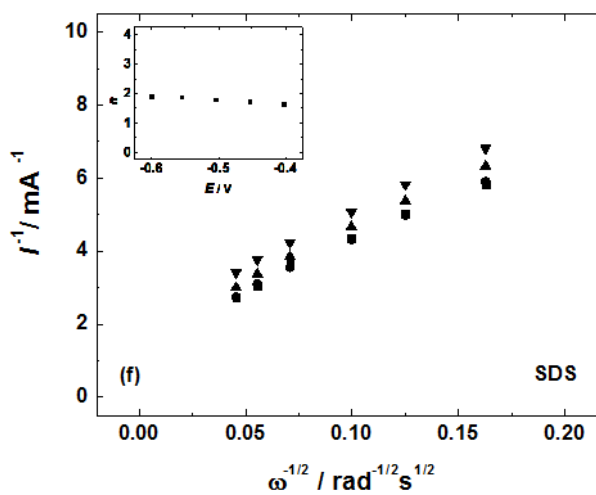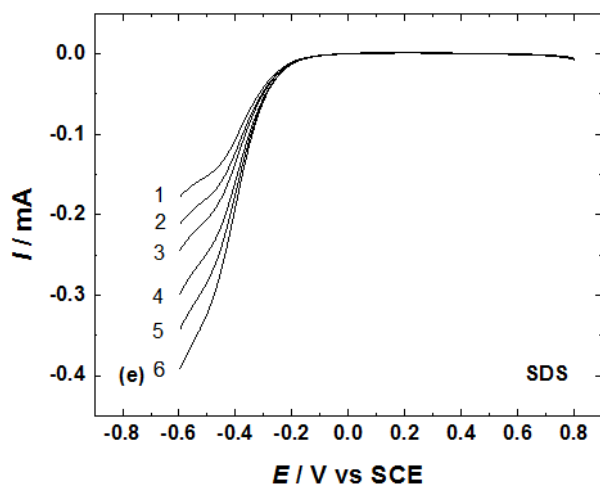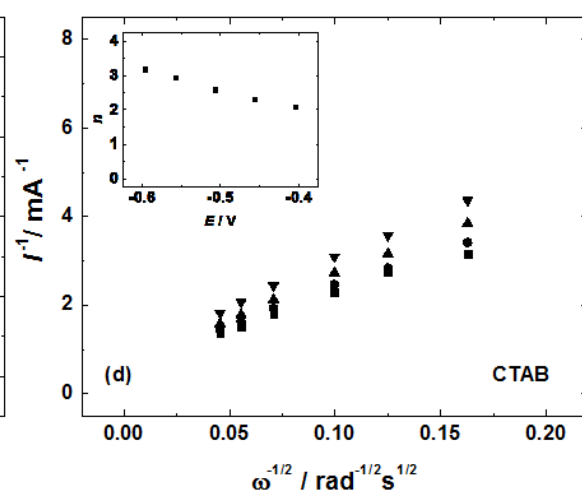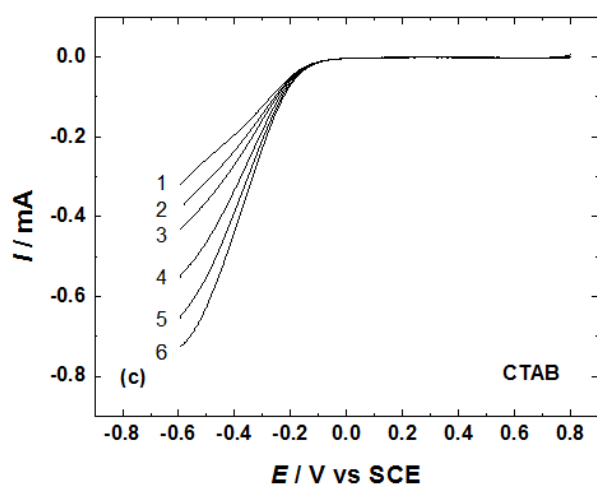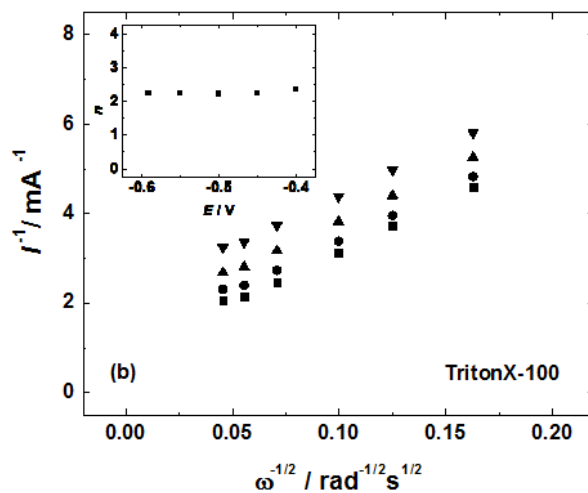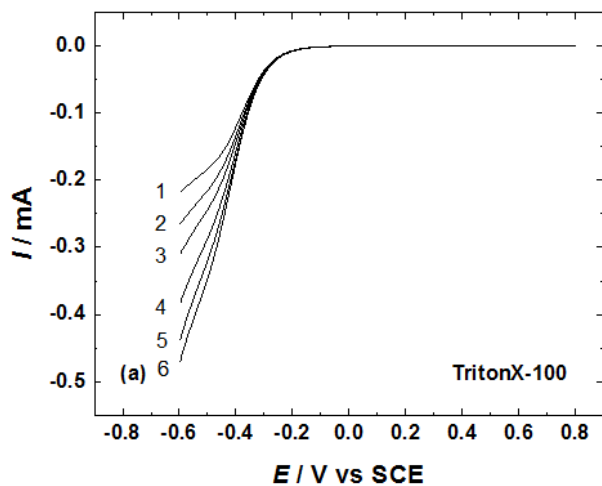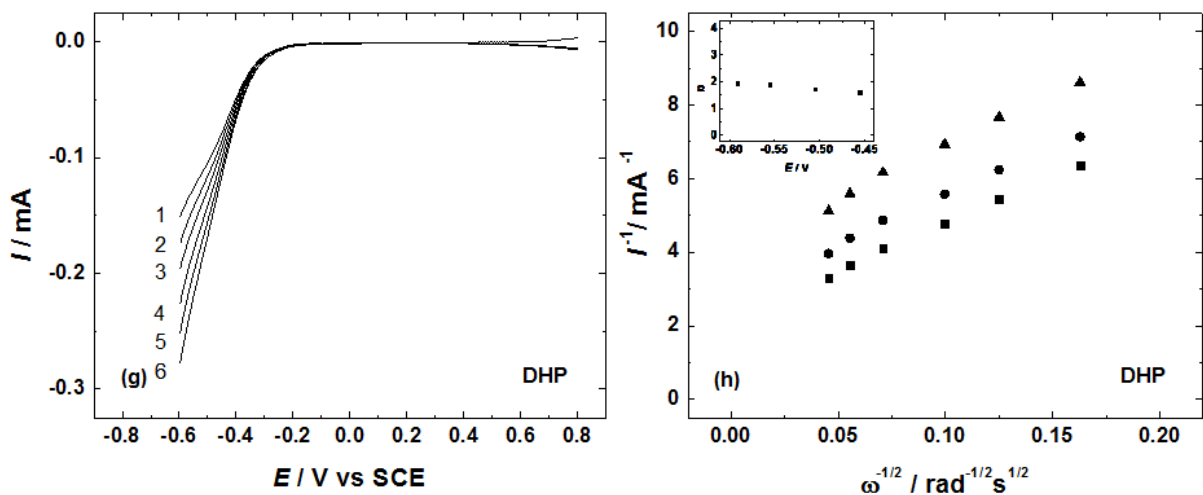
Figure 9. ORR polarisation curves and K-L plots for FWCNT-surfactant modified GC electrodes. Inset graphs show the potential dependence of the number of electrons transferred per O_2 molecule. Measurements were carried out in O_2 saturated 0.5 M H_2SO_4, v = 10 mV/s, ω = (1) 360, (2) 610, (3) 960, (4) 1900, (5) 3100, (6) 4600 rpm. In K-L plots symbols correspond to different potentials: (■) -0.6 V, (●) -0.55 V, (▲) -0.5 V, (▼) -0.45 V.

From Fig. 10 one can see that also in acid media carbon nanotubes modified with CTAB have the most positive onset potential and highest reduction current values. FWCNTs modified with DHP exhibit the lowest reduction current values and also have the most negative onset potential, indicating that using DHP the dispersion on FWCNTs was not enhanced.
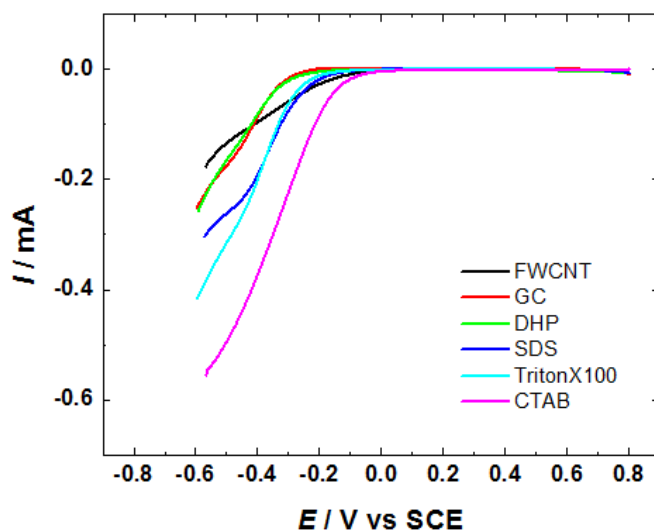
Figure 10. Comparison of the RDE voltammetry curves for ORR on a bare GC and on a FWCNT and FWCNT-surfactant modified GC electrodes. Measured in O_2 saturated 0.5 M H_2SO_4, v = 10 mV/s, ω = 1900 rpm.

5.3. Oxygen reduction on boron-doped carbon nanomaterial modified GC electrodes

5.3.1. Physical characteristics of boron-doped carbon nanomaterial

SEM was used to examine electrode surface after modification with boron-doped carbon nanomaterial. Fig. 11 presents SEM micrograph of a 1BC catalyst material. It can be seen that graphene flakes are evenly spread all over the material. It is possible to recognise some agglomeration of materials and also some restacking of graphene sheets.
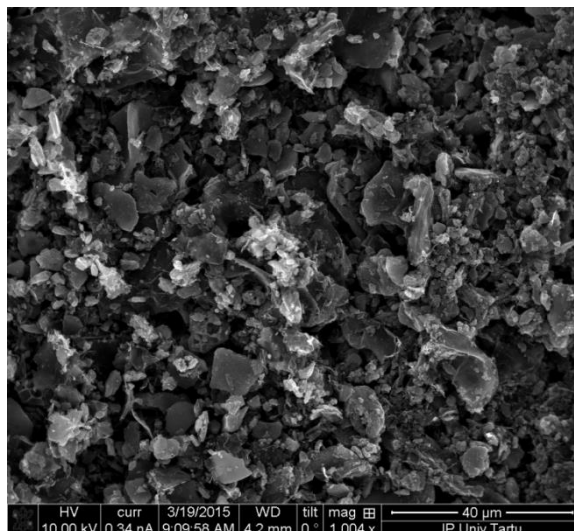
Figure 11. SEM image of a 1BC catalyst material.

Transmission electron microscopy (TEM) was used to explore carbon composite material structure and surface morphology after B-doping. While in some regions graphene flakes and nanotubes are well dispersed, it was also detected that in some regions restacking of graphene flakes takes place. From Fig. 12, it is possible to see graphene sheets cohered between the carbon nanotubes. In such way bigger restacking of the graphene to graphite is avoided. The current image shows approximately 4 layers of graphene together with FWCNTs, but it has been proven by the TEM study that there are regions where single-sheets are presented as well the areas where up to 8-layer graphene restacking has been taking place.
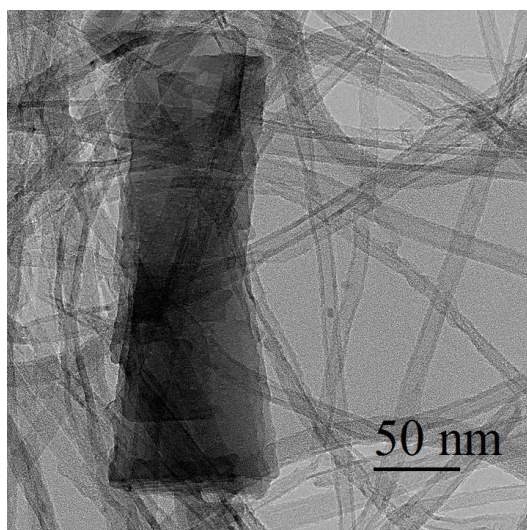
Figure 12. TEM image of B-doped graphene and CNTs. The image shows at least 4 layers of graphene with CNTs doing under and over the graphene sheets. Catalyst material 1BC was used for studying.

The graphitisation degree and ratio of carbon defects in the 1BC catalyst material were investigated by Raman spectroscopy. Fig. 13 illustrates that before B-doping the composite material exhibits an intense D and G peak at 1310 and 1584 cm^{-1}, respectively and after the B-doping D and G peak appear at 1303 and 1586 cm^{-1}, respectively. It is known that D band represents existence of sp^3 sites and G band sp^2 bonds. An intense D band indicates that a lot of defects have been created into carbon network during the acid treatment, leading to a sp^3 configuration. The ratio between D and G band intensities (I_D/I_G) is 1.69 for undoped carbon nanomaterial and 1.76 for B-doped carbon nanomaterial. While the bigger value indicates more defects it can be said that boron doping creates more imperfections.
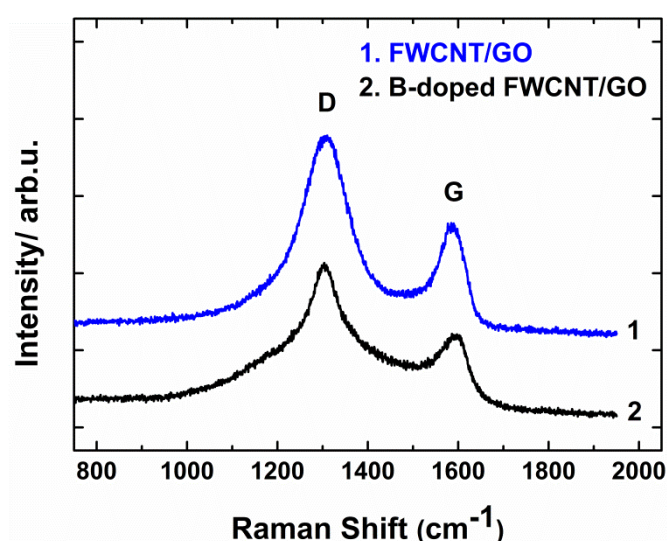
Figure 13. Raman spectra of FWCNT/GO and B-doped FWCNT/GO.

X-ray photoelectron spectroscopy (XPS) was used to study the surface chemical composition of the 1BC catalyst material. On Fig. 14 (a), the XPS survey spectra show the presence of boron, carbon, oxygen and fluorine atoms with atomic percentages of 1.7, 92, 6 and 0.6%, respectively. A distinguishable B1s peak appeared at 192.5 eV, C1s peak at 284 eV, O1s peak at 534.5 eV and F1s peak at 685.5 eV. C1s peak was deconvoluted into five separate peaks (see Fig. 14 (b)), C=C peak at 284 eV, B-C peak at 285 eV, C-C peak at 285.5 eV, C-O at 286.5 eV and O-C=O at 288.2 eV. On Fig. 14 (c), high resolution B1s XPS spectrum showed the appearance of three distinguishable peaks for different boron species, B_2O_3, BCO_2 and BC_2O at 193, 192.2 and 190.8 eV respectively. The proportion between different boron species is 60% of B_2O_3, 22% of BCO_2 and 18% of BC_2O. The binding energy of the B1s peak (192.5 eV) is positively shifted compared with pure boron binding energy (187.1 eV) [69]. This indicates that boron has been incorporated into carbon material by replacing C atoms in sp^2 carbon network.
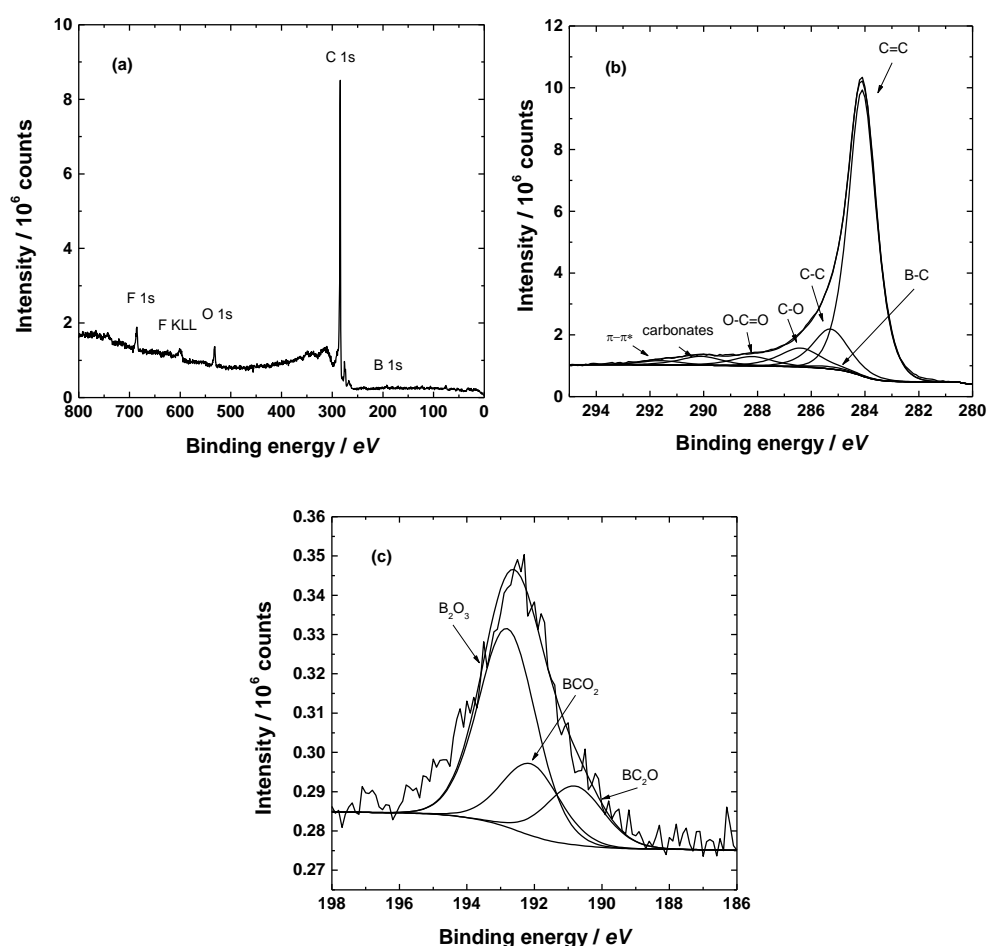
Figure 14. (a) XPS survey spectra of B-doped carbon material. High resolution XPS spectra in the C1s (b) and B1s (c) regions.

5.3.2. Electrochemical characterisation of boron-doped carbon nanomaterial modified electrodes

The rotating disk electrode method (RDE) was used to study the electrocatalytic activity of B-doped carbon nanomaterial towards O_2 electroreduction. Measurements were carried out in 0.1 M KOH solution and GC electrodes modified with B-doped carbon composite catalysts were used as working electrodes. In the first part four different mass ratios of carbon nanomaterial and boron source were prepared for pyrolysis process. Fig. 15 shows the RDE results for all four different mass ratios of boron source and carbon composite material at pyrolysis temperature at 800 °C.
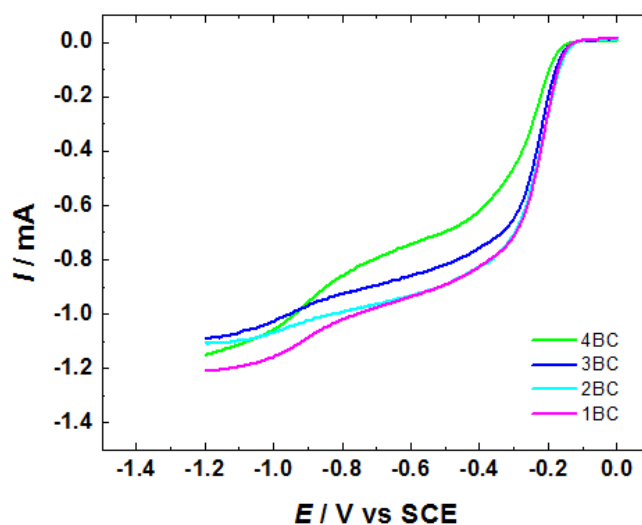
Figure 15. RDE voltammetry curves for ORR on a B-doped carbon nanomaterial with different mass ratios of boron source and carbon material (1BC, 2BC, 3BC and 4BC) in O_2 saturated 0.1 M KOH, $v = 10$ mV/s, $\omega = 1900$ rpm.

One can see that 1BC, 2BC and 3BC have the same onset potential which is approximately -0.15 V vs. SCE and is slightly more positive than for 4BC. The reduction current value is highest for catalyst material 1BC and lowest for 3BC and 4BC. These results indicate that increasing boron content decreases catalytic activity towards the ORR. Although some of the previous works show that increasing boron content the electrocatalytic activity of the material also increases, it should be mentioned that there are no previous works where BTDE has been used as a boron source for doping [46, 57]. It has been shown that in some point it will be rather difficult to increase boron content in carbon network just by increasing the amount of boron source [46]. Also defects and oxygen functional groups on carbon surface have important role in catalytic activity. Another reason for enhanced ORR activity of B-doped carbon is that by introducing boron into the material also oxygen reduction rate on catalyst material increases while boron atoms enhance oxygen adsorption [46]. It has been proposed

34

that positively charged boron atoms on carbon surface facilitate oxygen chemosorption and then act as a bridge from which electrons from the adjacent carbon atoms are transferred to oxygen leading the weakening of O-O bond [38].

The influence of pyrolysis temperature to electrocatalytic activity of the boron-doped material was investigated. While at 800 °C 1BC showed the best activity for ORR, the pyrolysis at temperatures 600 °C and 1000 °C were performed with the same boron source ratio to carbon material. In Fig. 16 one can see that catalyst material prepared by pyrolysis at 800 °C shows the best activity for O_2 reduction while having most positive onset potential and also largest reduction current value. From previous works it has been demonstrated that raising the temperature for doping increases the amount of electrocatalytically active surface species and therefore the material prepared at 800 °C is catalytically more active than the materials prepared at 600 °C [32, 59]. Although some of the previous reports have been demonstrating that 1000 °C is the most effective temperature for doping, raising temperature from 800 °C to 1000 °C, did not enhance the material catalytic activity towards the ORR in current work [46, 57]. Therefore using BTDE for boron-doping is more cost-effective than using boron sources which show the best result after doping at 1000 °C.
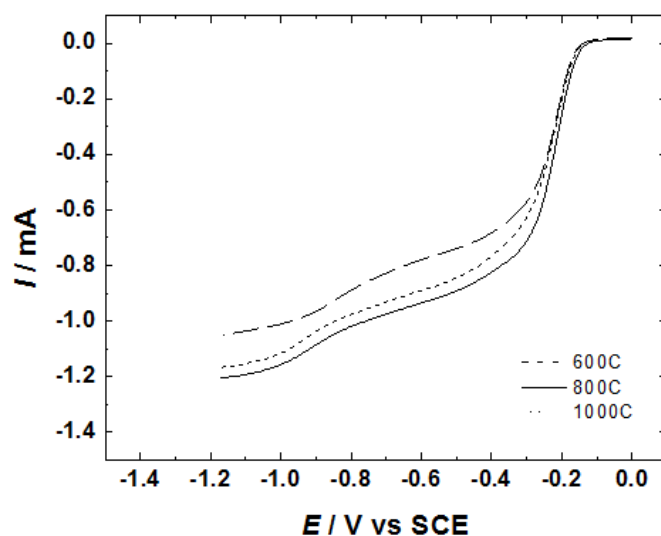
Figure 16. RDE voltammetry curves for ORR on a 1BC/GC electrode prepared at pyrolysis temperatures 600, 800 and 1000 °C in O_2 saturated 0.1 M KOH, $v = 10$ mV/s, $\omega = 1900$ rpm.

Fig. 17 illustrates a set of ORR polarisation curves measured at different rotation rates on most active, 1BC catalyst modified GC electrode. The onset potential is approximately -0.15 V vs SCE and at lower rotating rates reduction current plateaus are formed indicating that the ORR process is almost entirely under the diffusion control. At higher rotating speeds slight

prewave is formed at -0.8 V. This behaviour is common to carbon materials in alkaline solution and can be suggested that it is contributed by the oxygen groups on the surface [70]. The number of electrons transferred per O_2 molecule was calculated using the K-L equation (15). From Fig. 18 it can be seen that the intercepts on a K-L plot are close to zero which indicates that ORR is almost entirely under the diffusion control. The number of electrons transferred per O_2 molecule is close to four in all over the measured potential range, indicating that on these B-doped carbon composite catalysts a four-electron reduction pathway is preferred over two-electron reduction pathway.
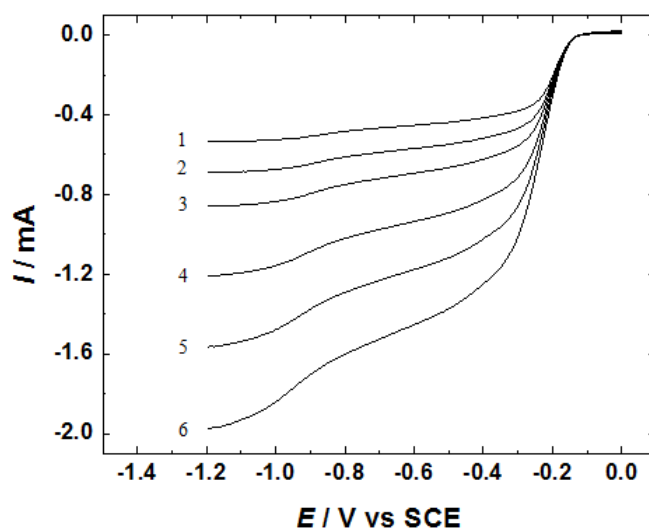
Figure 17. RDE voltammetry curves for ORR on a 1BC/GC electrode in O_2 saturated 0.1 M KOH, $\upsilon = 10$ mV/s, $\omega =$ (1) 360, (2) 610, (3) 960, (4) 1900, (5) 3100, (6) 4600 rpm.
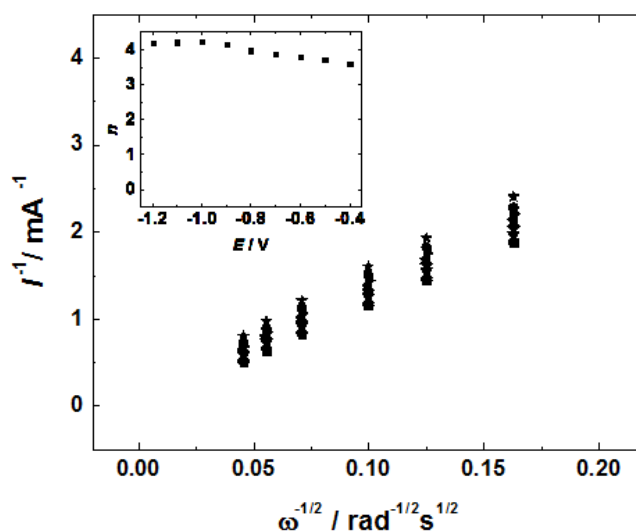
Figure 18. K-L plots for oxygen reduction on a 1BC/GC electrode in O_2 saturated 0.1 M KOH. Inset shows the potential dependence of the number of electrons transferred per O_2 molecule. Data derived from Fig. 17. In K-L plots symbols correspond to different potentials: (■) -1.2 V, (⬟) -1.1 V, (▲) -1.0 V, (▼) -0.9 V, (◆) -0.8 V, (◀) -0.7 V, (▶) -0.6 V, (●) -0.5 V, (★) -0.4 V.

From Fig. 19, it can be seen that the mixture of GO and acid treated FWCNT have more positive onset potential compared with GC. After the boron doping onset potential shifts even more positive, half-wave potential value is approximately 200 mV more positive compared with bare GC and also reduction current values have increased. For that reason it can be said that boron atoms have been incorporated into carbon network and by that electronic properties of the material have been changed.
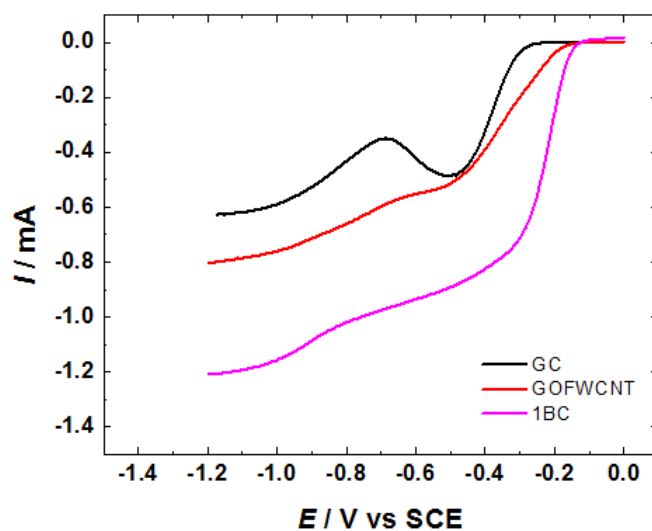
Figure 19. RDE voltammetry curves for ORR on a bare GC, GC modified with GO/FWCNT and 1BC/GC in O_2 saturated 0.1 M KOH, v = 10 mV/s, ω = 1900 rpm.

6. Summary

The dispersion of few-walled carbon nanotubes (FWCNTs) was enhanced in the presence of surfactant. This was proven by the increase of reduction current values which indicates that the specific surface area of the electrode has been increased. Comparison was made with un-modified FWCNTs which electrocatalytic activity was measured using RRDE method. Four different surfactants were used for modification (Triton X-100, CTAB, SDS and DHP). The best dispersibility has been shown by using a cationic surfactant CTAB. Electrocatalytic activity of surfactant modified FWCNTs decreased when the pH value of electrolyte decreased. It can be suggested that at very low pH values the studied material can be used as a catalyst support.

In the second part of the thesis boron-doped carbon nanomaterials were successfully produced by using FWCNTs and graphene oxide (GO) mixture as a composite material and boron trifluoride diethyl etherate (BTDE) as a boron source. Four different mass ratios (1/5, 1/10, 1/20, 1/40) of carbon composite and boron source were studied and the best catalytic activity was shown by the catalyst with carbon material and boron source mass ratio of 1/5. In this work it was demonstrated that by increasing boron source for doping the catalytic activity of material decreased. Although this result is contemporary to some of the previous works it has to be mentioned that BTDE has not been used as a boron source for doping in previous reports. The effect of pyrolysis temperature on the electrocatalytic activity was also examined. Pyrolysis was carried out using temperatures 600, 800 and 1000 °C. The most electrocatalytically active material was produced at pyrolysis temperature of 800 °C. Although some previous works have been shown that by increasing pyrolysis temperature the catalytic activity has also been enhanced, it this work raising temperature from 800 °C to 1000 °C the catalytic activity of the material did not improve. Therefore it can be said that using BTDE as a boron source for doping is rather easy and cost-effective way to improve carbon nanomaterial electrocatalytic activity towards O_2 electroreduction. The resulting catalyst material exhibited excellent electrocatalytic activity towards the ORR in alkaline media. This indicates that the synthesised B-doped catalyst material is promising for widespread electrochemical applications, especially for anion-exchange membrane fuel cells.

7. Résumé

For large scale production of low-temperature fuel cells, cathode catalyst for efficient oxygen reduction reaction (ORR) is needed. At present mostly platinum based catalysts are used, but due to high price of platinum and other drawbacks like sensitivity towards impurities, an alternative catalyst material is needed. In current study surfactant coated few-walled carbon nanotubes and boron-doped carbon nanomaterial were prepared and the electrocatalytic activity towards the ORR was studied on both as-prepared catalysts. In addition for electrochemical measurements also surface characterisation were carried out using scanning electron microscopy (SEM), transmission electron microscopy (TEM), Raman spectroscopy and X-ray photoelectron spectroscopy (XPS). For electrochemical measurements the rotating disk electrode (RDE) and rotating ring-disk electrode (RRDE) methods were used. With boron-doped carbon nanomaterial the RDE experiments were carried out in 0.1 M KOH solution and with surfactant-modified carbon nanotubes measurements in 0.1 M KOH solution as well as in 0.1 M phosphate buffer and in 0.5 M H_2SO_4 media were performed.

It has been demonstrated that in the presence of surfactant the specific surface area of carbon nanotubes has been increased while current values were higher compared with non-modified carbon nanotubes. The activity towards the ORR was much lower in acid solutions and it can be suggested that this carbon nanotube catalyst material could act as a catalyst support in certain potential range in acid media, while having a good conductivity but does not contribute to ORR itself.

For boron-doped carbon nanomaterial, boron trifluoride diethyl etherate (BTDE) was used as a boron source. XPS spectra demonstrated that boron has been successfully incorporated into carbon network. Raman spectroscopy showed slight increase in the ratio between D and G band intensities (I_D/I_G), which indicates that more defects have been introduced into material after doping. Electrochemical measurements with four different mass ratios of carbon composite and boron source (FWCNT and GO/boron source = 1/5, 1/10, 1/20 and 1/40) were carried out. Electrocatalytically most active was the material with carbon composite and boron source mass ratio of 1/5. The effect of pyrolysis temperature on the electrocatalytic activity of the boron-doped material was also investigated. Pyrolysis at temperatures 600, 800 and 1000 °C were performed and the material prepared at 800 °C showed the best activity for O_2 electroreduction. It can be proposed that using BTDE for introducing boron into carbon network is effective and rather easy way to enhance the ORR activity of carbon nanomaterial.

8. Resümee

Energia muundamissüsteemides, nagu näiteks madaltemperatuuriline kütuseelement ja metall-õhk patareid, on üks olulisemaid protsesse hapniku elektroredutseerimine, mis leiab aset katoodil. Kütuseelemendi aktiivsus on otseselt seotud hapniku redutseerumise kineetikaga, seega on oluline, et antud reaktsioon toimuks võimalikult kiiresti. Kahjuks aga on O=O sideme lõhkumiseks vaja kulutada palju energiat ja seega on O_2 elektroredutseerumine pigem aeglane. Protsessi kiirendamiseks on vaja efektiivset katalüsaatorit kütuseelemendi katoodi poolele. Hetkel on enamlevinud katalüsaatorid valmistatud plaatina baasil, mis on kallis ja tundlik kütuses leiduvatele lisanditele nagu näiteks väävel ja süsinikdioksiid. Antud töös uuriti modifitseeritud süsiniknanomaterjalide mõju hapniku elektroredutseerumisele. Töö koosnes kahest osast, milles esimeses modifitseeriti mõneseinalisi süsiniknanotorusid nelja erineva pindaktiivse ainega, et saavutada nanotorude parem dispergeeritus. Võib väita, et nanotorude dispergeeritavus paranes pindaktiivse ainete juuresolekul. Seda illustreeris polarisatsiooni kõveratel suurenenud vooluväärtused võrreldes ilma pindaktiivse aineta süsinikmaterjali *I,E*-kõveratega, see tähendab, et elektroodi eripinda suurendati. Parima dispergeeritavuse tagas katioonne pindaktiivne aine tsetüültrimetüülammoonium bromiid (CTAB).

Töö teises osas valmistati booriga dopeeritud süsiniknanomaterjalid ja uuriti nende mõju hapniku elektroredutseerumisele. Süsiniknanomaterjalina kasutati mõneseinaliste süsiniknanotorude ja grafeenoksiidi suhtega 1:1 segu ja boori allikana boortrifluoriiddietüületeraati (BTDE). Valmistati neli erineva süsinik komposiitmaterjali ja boori allika massi suhtega katalüsaatormaterjali. Katalüütiliselt kõige aktiivsemaks osutus materjal, mille süsiniknanomaterjali ja boori allika suhe oli vastavalt 1/5. Uuriti ka pürolüüsitemperatuuri mõju booriga dopeeritud süsiniknanomaterjalide elektrokatalüütilisele aktiivsusele. Dopeerimised teostati temperatuuridel 600, 800 ja 1000 °C. Katalüütiliselt kõige aktiivsem aine saadi dopeerides 800 °C juures. See annab antud ainele (BTDE) teatud eelise boori allikate ees, mis annavad kõige efektiivsema tulemuse 1000 °C juures.

9. References

[1] J. Zhang, PEM Fuel Cell Electrocatalysts and Catalyst Layers: Fundamentals and Applications, Springer, London, 2008.

[2] W. Xing, G. Yin, J. Zhang, Rotating Electrode Methods and Oxygen Reduction Electrocatalysts, Elsevier, Amsterdam, 2014.

[3] B.E. Conway, J. O`M. Bockris, E. Yeager, Comprehensive Treatise of Electrochemistry. Vol.7. Kinetics and Mechanisms of Electrode Processes, Plenum Press, New York, 1983.

[4] A.J. Bard, L.R. Faulkner, Electrochemical Methods: Fundamentals and Applications, 2nd ed., Wiley, New York, 2001.

[5] H.H. Yang, R.L. McCreery, Elucidation of the Mechanism of Dioxygen Reduction on Metal-Free Carbon Electrodes, Journal of The Electrochemical Society, 147 (2000) 3420-3428.

[6] D.A. Tryk, C.R. Cabrera, A. Fujishima, N. Spataru, Oxygen electroreduction on carbon materials, in: J. Prakash, D. Chu, D. Scherson, M. Enayetullah, I. Tae Bae (Eds.), Fundamental Understanding of Electrode Processes in Memory of Professor Ernest B. Yeager, The Electrochemical Society Proceedings, Pennington, New Jersey, 2005, 45–57.

[7] R.J. Taylor, A.A. Humffray, Electrochemical studies on glassy carbon electrodes: II. Oxygen reduction in solutions of high pH (pH>10), Journal of Electroanalytical Chemistry and Interfacial Electrochemistry, 64 (1975) 63-84.

[8] C. Paliteiro, A. Hamnett, J.B. Goodenough, The electroreduction of oxygen on pyrolytic graphite, Journal of Electroanalytical Chemistry and Interfacial Electrochemistry, 233 (1987) 147-159.

[9] R.J. Taylor, A.A. Humffray, Electrochemical studies on glassy carbon electrodes: IV. Influence of solution pH and buffer capacity on reduction of oxygen, Journal of Electroanalytical Chemistry and Interfacial Electrochemistry, 64 (1975) 95-105.

[10] M.S. Hossain, D. Tryk, E. Yeager, The electrochemistry of graphite and modified graphite surfaces: the reduction of O2, Electrochimica Acta, 34 (1989) 1733-1737.

[11] K. Tammeveski, K. Kontturi, R.J. Nichols, R.J. Potter, D.J. Schiffrin, Surface redox catalysis for O2 reduction on quinone-modified glassy carbon electrodes, Journal of Electroanalytical Chemistry, 515 (2001) 101-112.

[12] A. Sarapuu, K. Helstein, D.J. Schiffrin, K. Tammeveski, Kinetics of Oxygen Reduction on Quinone-Modified HOPG and BDD Electrodes in Alkaline Solution, Electrochemical and Solid-State Letters, 8 (2005) E30-E33.

[13] K. Vaik, A. Sarapuu, K. Tammeveski, F. Mirkhalaf, D.J. Schiffrin, Oxygen reduction on phenanthrenequinone-modified glassy carbon electrodes in 0.1 M KOH, Journal of Electroanalytical Chemistry, 564 (2004) 159-166.

[14] A. Sarapuu, K. Vaik, D.J. Schiffrin, K. Tammeveski, Electrochemical reduction of oxygen on anthraquinone-modified glassy carbon electrodes in alkaline solution, Journal of Electroanalytical Chemistry, 541 (2003) 23-29.

[15] M. Zhang, Y. Yan, K. Gong, L. Mao, Z. Guo, Y. Chen, Electrostatic Layer-by-Layer Assembled Carbon Nanotube Multilayer Film and Its Electrocatalytic Activity for O2 Reduction, Langmuir, 20 (2004) 8781-8785.

[16] K. Matsubara, K. Waki, The Effect of the Oxygen-Containing Functional Groups on the Electrochemical Reduction of Oxygen of Multi-Walled Carbon Nanotubes in Acid Media, ECS Transactions, 28 (2010) 35-46.

[17] M. Carmo, V.A. Paganin, J.M. Rosolen, E.R. Gonzalez, Alternative supports for the preparation of catalysts for low-temperature fuel cells: the use of carbon nanotubes, Journal of Power Sources, 142 (2005) 169-176.

[18] G. Che, B.B. Lakshmi, E.R. Fisher, C.R. Martin, Carbon nanotubule membranes for electrochemical energy storage and production, Nature, 393 (1998) 346-349.

[19] Y. Xu, H. Bai, G. Lu, C. Li, G. Shi, Flexible Graphene Films via the Filtration of Water-Soluble Noncovalent Functionalized Graphene Sheets, Journal of the American Chemical Society, 130 (2008) 5856-5857.

[20] C. Zhu, S. Dong, Recent progress in graphene-based nanomaterials as advanced electrocatalysts towards oxygen reduction reaction, Nanoscale, 5 (2013) 1753-1767.

[21] J. Yan, T. Wei, B. Shao, F. Ma, Z. Fan, M. Zhang, C. Zheng, Y. Shang, W. Qian, F. Wei, Electrochemical properties of graphene nanosheet/carbon black composites as electrodes for supercapacitors, Carbon, 48 (2010) 1731-1737.

[22] C. Zhong, J.-Z. Wang, D. Wexler, H.-K. Liu, Microwave autoclave synthesized multi-layer graphene/single-walled carbon nanotube composites for free-standing lithium-ion battery anodes, Carbon, 66 (2014) 637-645.

[23] L.-H. Chang, C.-K. Hsieh, M.-C. Hsiao, J.-C. Chiang, P.-I. Liu, K.-K. Ho, C.-C.M. Ma, M.-Y. Yen, M.-C. Tsai, C.-H. Tsai, A graphene-multi-walled carbon nanotube hybrid supported on fluorinated tin oxide as a counter electrode of dye-sensitized solar cells, Journal of Power Sources, 222 (2013) 518-525.

[24] Y.-S. Wang, S.-Y. Yang, S.-M. Li, H.-W. Tien, S.-T. Hsiao, W.-H. Liao, C.-H. Liu, K.-H. Chang, C.-C.M. Ma, C.-C. Hu, Three-dimensionally porous graphene–carbon nanotube

composite-supported PtRu catalysts with an ultrahigh electrocatalytic activity for methanol oxidation, Electrochimica Acta, 87 (2013) 261-269.

[25] Z. Fan, J. Yan, L. Zhi, Q. Zhang, T. Wei, J. Feng, M. Zhang, W. Qian, F. Wei, A Three-Dimensional Carbon Nanotube/Graphene Sandwich and Its Application as Electrode in Supercapacitors, Advanced Materials, 22 (2010) 3723-3728.

[26] C. Arbizzani, S. Righi, F. Soavi, M. Mastragostino, Graphene and carbon nanotube structures supported on mesoporous xerogel carbon as catalysts for oxygen reduction reaction in proton-exchange-membrane fuel cells, International Journal of Hydrogen Energy, 36 (2011) 5038-5046.

[27] C.H. Choi, M.W. Chung, H.C. Kwon, J.H. Chung, S.I. Woo, Nitrogen-doped graphene/carbon nanotube self-assembly for efficient oxygen reduction reaction in acid media, Applied Catalysis B: Environmental, 144 (2014) 760-766.

[28] S. Ratso, I. Kruusenberg, M. Vikkisk, U. Joost, E. Shulga, I. Kink, T. Kallio, K. Tammeveski, Highly active nitrogen-doped few-layer graphene/carbon nanotube composite electrocatalyst for oxygen reduction reaction in alkaline media, Carbon, 73 (2014) 361-370.

[29] C.H. Choi, S.H. Park, S.I. Woo, Binary and Ternary Doping of Nitrogen, Boron, and Phosphorus into Carbon for Enhancing Electrochemical Oxygen Reduction Activity, ACS Nano, 6 (2012) 7084-7091.

[30] S. Zhong, L. Zhou, L. Wu, L. Tang, Q. He, J. Ahmed, Nitrogen- and boron-co-doped core–shell carbon nanoparticles as efficient metal-free catalysts for oxygen reduction reactions in microbial fuel cells, Journal of Power Sources, 272 (2014) 344-350.

[31] Z.-H. Sheng, H.-L. Gao, W.-J. Bao, F.-B. Wang, X.-H. Xia, Synthesis of boron doped graphene for oxygen reduction reaction in fuel cells, Journal of Materials Chemistry, 22 (2012) 390-395.

[32] G. Jo, S. Shanmugam, Single-step synthetic approach for boron-doped carbons as a non-precious catalyst for oxygen reduction in alkaline medium, Electrochemistry Communications, 25 (2012) 101-104.

[33] M. Endo, H. Muramatsu, T. Hayashi, Y.-A. Kim, G.V. Lier, J.-C. Charlier, H. Terrones, M. Terrones, M.S. Dresselhaus, Atomic Nanotube Welders: Boron Interstitials Triggering Connections in Double-Walled Carbon Nanotubes, Nano Letters, 5 (2005) 1099-1105.

[34] K. McGuire, N. Gothard, P.L. Gai, M.S. Dresselhaus, G. Sumanasekera, A.M. Rao, Synthesis and Raman characterization of boron-doped single-walled carbon nanotubes, Carbon, 43 (2005) 219-227.

[35] J. Maultzsch, S. Reich, C. Thomsen, S. Webster, R. Czerw, D.L. Carroll, S.M.C. Vieira, P.R. Birkett, C.A. Rego, Raman characterization of boron-doped multiwalled carbon nanotubes, Applied physics letters, 81 (2002) 2647-2649.

[36] S. Shiraishi, M. Kibe, T. Yokoyama, H. Kurihara, N. Patel, A. Oya, Y. Kaburagi, Y. Hishiyama, Electric double layer capacitance of multi-walled carbon nanotubes and B-doping effect, Applied Physics A, 82 (2006) 585-591.

[37] H. Mousavi, R. Moradian, Nitrogen and boron doping effects on the electrical conductivity of graphene and nanotube, Solid State Sciences, 13 (2011) 1459-1464.

[38] L. Yang, S. Jiang, Y. Zhao, L. Zhu, S. Chen, X. Wang, Q. Wu, J. Ma, Y. Ma, Z. Hu, Boron-Doped Carbon Nanotubes as Metal-Free Electrocatalysts for the Oxygen Reduction Reaction, Angewandte Chemie International Edition, 50 (2011) 7132-7135.

[39] K. Gong, F. Du, Z. Xia, M. Durstock, L. Dai, Nitrogen-Doped Carbon Nanotube Arrays with High Electrocatalytic Activity for Oxygen Reduction, Science, 323 (2009) 760-764.

[40] X. Hu, Y. Wu, H. Li, Z. Zhang, Adsorption and Activation of O2 on Nitrogen-Doped Carbon Nanotubes, The Journal of Physical Chemistry C, 114 (2010) 9603-9607.

[41] M. Grujicic, G. Cao, A.M. Rao, T.M. Tritt, S. Nayak, UV-light enhanced oxidation of carbon nanotubes, Applied Surface Science, 214 (2003) 289-303.

[42] Y. Liu, S. Chen, X. Quan, H. Yu, H. Zhao, Y. Zhang, G. Chen, Boron and Nitrogen Codoped Nanodiamond as an Efficient Metal-Free Catalyst for Oxygen Reduction Reaction, The Journal of Physical Chemistry C, 117 (2013) 14992-14998.

[43] P. Lazar, R. Zboril, M. Pumera, M. Otyepka, Chemical nature of boron and nitrogen dopant atoms in graphene strongly influences its electronic properties, Physical Chemistry Chemical Physics, 16 (2014) 14231-14235.

[44] T. Kondo, Y. Kodama, S. Ikezoe, K. Yajima, T. Aikawa, M. Yuasa, Porous boron-doped diamond electrodes fabricated via two-step thermal treatment, Carbon, 77 (2014) 783-789.

[45] G. Fazio, L. Ferrighi, C. Di Valentin, Boron-doped graphene as active electrocatalyst for oxygen reduction reaction at a fuel-cell cathode, Journal of Catalysis, 318 (2014) 203-210.

[46] Y. Cheng, Y. Tian, X. Fan, J. Liu, C. Yan, Boron Doped Multi-walled Carbon Nanotubes as Catalysts for Oxygen Reduction Reaction and Oxygen Evolution Reactionin in Alkaline Media, Electrochimica Acta, 143 (2014) 291-296.

[47] W. Xia, J. Masa, M. Bron, W. Schuhmann, M. Muhler, Highly active metal-free nitrogen-containing carbon catalysts for oxygen reduction synthesized by thermal treatment of polypyridine-carbon black mixtures, Electrochemistry Communications, 13 (2011) 593-596.

[48] M. Vikkisk, I. Kruusenberg, U. Joost, E. Shulga, K. Tammeveski, Electrocatalysis of oxygen reduction on nitrogen-containing multi-walled carbon nanotube modified glassy carbon electrodes, Electrochimica Acta, 87 (2013) 709-716.

[49] H. Li, W. Kang, L. Wang, Q. Yue, S. Xu, H. Wang, J. Liu, Synthesis of three-dimensional flowerlike nitrogen-doped carbons by a copyrolysis route and the effect of nitrogen species on the electrocatalytic activity in oxygen reduction reaction, Carbon, 54 (2013) 249-257.

[50] N. Alexeyeva, E. Shulga, V. Kisand, I. Kink, K. Tammeveski, Electroreduction of oxygen on nitrogen-doped carbon nanotube modified glassy carbon electrodes in acid and alkaline solutions, Journal of Electroanalytical Chemistry, 648 (2010) 169-175.

[51] H. Liu, Y. Liu, D. Zhu, Chemical doping of graphene, Journal of Materials Chemistry, 21 (2011) 3335-3345.

[52] L. Lai, J.R. Potts, D. Zhan, L. Wang, C.K. Poh, C. Tang, H. Gong, Z. Shen, J. Lin, R.S. Ruoff, Exploration of the active center structure of nitrogen-doped graphene-based catalysts for oxygen reduction reaction, Energy & Environmental Science, 5 (2012) 7936-7942.

[53] Z.-W. Liu, F. Peng, H.-J. Wang, H. Yu, W.-X. Zheng, J. Yang, Phosphorus-Doped Graphite Layers with High Electrocatalytic Activity for the O2 Reduction in an Alkaline Medium, Angewandte Chemie International Edition, 50 (2011) 3257-3261.

[54] J. Liu, P. Song, Z. Ning, W. Xu, Recent Advances in Heteroatom-Doped Metal-Free Electrocatalysts for Highly Efficient Oxygen Reduction Reaction, Electrocatalysis, 6 (2015) 132-147.

[55] Y. Jiao, Y. Zheng, M. Jaroniec, S.Z. Qiao, Origin of the Electrocatalytic Oxygen Reduction Activity of Graphene-Based Catalysts: A Roadmap to Achieve the Best Performance, Journal of the American Chemical Society, 136 (2014) 4394-4403.

[56] Z. Yang, H. Nie, X.a. Chen, X. Chen, S. Huang, Recent progress in doped carbon nanomaterials as effective cathode catalysts for fuel cell oxygen reduction reaction, Journal of Power Sources, 236 (2013) 238-249.

[57] X. Bo, M. Li, C. Han, L. Guo, The influence of boron dopant on the electrochemical properties of graphene as an electrode material and a support for Pt catalysts, Electrochimica Acta, 114 (2013) 582-589.

[58] T. Hagio, M. Nakamizo, K. Kobayashi, Studies on X-ray diffraction and Raman spectra of B-doped natural graphite, Carbon, 27 (1989) 259-263.

[59] X. Xu, T. Yuan, Y. Zhou, Y. Li, J. Lu, X. Tian, D. Wang, J. Wang, Facile synthesis of boron and nitrogen-doped graphene as efficient electrocatalyst for the oxygen reduction

reaction in alkaline media, International Journal of Hydrogen Energy, 39 (2014) 16043-16052.

[60] K.L. Lu, R.M. Lago, Y.K. Chen, M.L.H. Green, P.J.F. Harris, S.C. Tsang, Mechanical damage of carbon nanotubes by ultrasound, Carbon, 34 (1996) 814-816.

[61] J. Hilding, E.A. Grulke, Z. George Zhang, F. Lockwood, Dispersion of Carbon Nanotubes in Liquids, Journal of Dispersion Science and Technology, 24 (2003) 1-41.

[62] A.R. Blythe, D. Bloor, Electrical Properties of Polymers, Cambridge University Press, 2005.

[63] R. Rastogi, R. Kaushal, S.K. Tripathi, A.L. Sharma, I. Kaur, L.M. Bharadwaj, Comparative study of carbon nanotube dispersion using surfactants, Journal of Colloid and Interface Science, 328 (2008) 421-428.

[64] I. Kruusenberg, N. Alexeyeva, K. Tammeveski, The pH-dependence of oxygen reduction on multi-walled carbon nanotube modified glassy carbon electrodes, Carbon, 47 (2009) 651-658.

[65] J. Yu, N. Grossiord, C.E. Koning, J. Loos, Controlling the dispersion of multi-wall carbon nanotubes in aqueous surfactant solution, Carbon, 45 (2007) 618-623.

[66] V.S. Bagotsky, Fundamentals of Electrochemistry, Wiley, New York, 2005.

[67] W.S. Hummers, R.E. Offeman, Preparation of Graphitic Oxide, Journal of the American Chemical Society, 80 (1958) 1339-1339.

[68] L. Sun, L. Wang, C. Tian, T. Tan, Y. Xie, K. Shi, M. Li, H. Fu, Nitrogen-doped graphene with high nitrogen level via a one-step hydrothermal reaction of graphene oxide with urea for superior capacitive energy storage, RSC Advances, 2 (2012) 4498-4506.

[69] M. Sankaran, B. Viswanathan, Hydrogen storage in boron substituted carbon nanotubes, Carbon, 45 (2007) 1628-1635.

[70] Z.-H. Sheng, L. Shao, J.-J. Chen, W.-J. Bao, F.-B. Wang, X.-H. Xia, Catalyst-Free Synthesis of Nitrogen-Doped Graphene via Thermal Annealing Graphite Oxide with Melamine and Its Excellent Electrocatalysis, ACS Nano, 5 (2011) 4350-4358.